INL EXT-21-63502

Laser-based Adhesion Strength Measurements for Advanced Manufactured Sensor Adhesion Characterization

July 2021

Advanced Sensors and Instrumentation Program

Amey R. Khanolkar
Energy and Environment Science and Technology, Idaho National Laboratory

Kiyo T. Fujimoto
Energy and Environment Science and Technology, Idaho National Laboratory

Michael D. McMurtrey
Nuclear Science and Technology, Idaho National Laboratory

Idaho National Laboratory

INL is a U.S. Department of Energy National Laboratory
operated by Battelle Energy Alliance, LLC

DISCLAIMER

This information was prepared as an account of work sponsored by an agency of the U.S. Government. Neither the U.S. Government nor any agency thereof, nor any of their employees, makes any warranty, expressed or implied, or assumes any legal liability or responsibility for the accuracy, completeness, or usefulness, of any information, apparatus, product, or process disclosed, or represents that its use would not infringe privately owned rights. References herein to any specific commercial product, process, or service by trade name, trade mark, manufacturer, or otherwise, does not necessarily constitute or imply its endorsement, recommendation, or favoring by the U.S. Government or any agency thereof. The views and opinions of authors expressed herein do not necessarily state or reflect those of the U.S. Government or any agency thereof.

INL EXT-21-63502

Laser-based Adhesion Strength Measurements for Advanced Manufactured Sensor Adhesion Characterization

Advanced Sensors and Instrumentation Program

Amey R. Khanolkar
Energy and Environment Science and Technology, Idaho National Laboratory
Kiyo T. Fujimoto
Energy and Environment Science and Technology, Idaho National Laboratory
Michael D. McMurtrey
Nuclear Science and Technology, Idaho National Laboratory

July 2021

Idaho National Laboratory
Idaho Falls, Idaho 83415

http://www.inl.gov

Prepared for the
U.S. Department of Energy
Office of Nuclear Energy
Under DOE Idaho Operations Office
Contract DE-AC07-05ID14517

Page intentionally left blank

ABSTRACT

As part of the advanced manufacturing (AM) focus of the Nuclear Energy Enabling Technologies Advanced Sensors and Instrumentation Program, new in-house capabilities to fabricate and test novel active and passive in-pile sensors are being developed at Idaho National Laboratory (INL). These advanced manufactured sensors, such as peak temperature monitors and strain gauges, must be miniaturized and be able to provide real-time feedback, all while withstanding the coupled extremes of temperature and radiation typically observed in the environment of a nuclear test reactor. Fabricating durable and robust in-pile sensors with high fidelity requires a fundamental understanding of the optimal process parameters required in the AM technique, as well as the effect of deviations from optimal process parameters on the sensor-substrate adhesion and the ultimate robustness of the sensor. This report presents the use of a laser-based, non-contact approach for characterizing the adhesion of sensors manufactured using aerosol jet printing (AJP) that is comprised of silver nanoparticle inks deposited and sintered on austenitic stainless steel 316L substrates. The effect of substrate surface roughness, surface energy, ink sintering time and sintering temperature on the printed sensor topography, and the sensor-substrate adhesion has been systematically investigated. The sensor-substrate interfacial adhesion strength was determined from the critical laser pulse energy required to ablate/detach the printed sensor from the substrate. Measurements of the sensor topography using optical profilometry revealed that post-deposition sintering at 400°C for 60 minutes resulted in a reduced sensor thickness, while plasma treating the substrate prior to printing yielded sensors with uniform thickness profiles transverse to the print direction. Sintering temperature and time were found to be the dominant parameters that affected sensor-substrate adhesion, followed by substrate surface roughness. The laser-based and locally destructive approach for adhesion strength measurements shows promise in overcoming the challenges and limitations of current standardized peel tests and can be developed into a post-fabrication process control protocol for evaluating the durability of AM-printed sensors in a high-throughput fashion. Future studies will investigate the use of laser-induced spallation techniques as well as non-destructive laser ultrasonic methods for sensor-substrate adhesion characterization on sensors manufactured using AJP and other AM techniques, such as plasma jet printing.

Page intentionally left blank

ACKNOWLEDGEMENTS

The authors would like to thank Richard Hatch and Eric Lumley from the INL Fabrication Services Department for their assistance in machining the stainless steel substrates used in this study, as well as Wesley Jones from the INL Materials Science and Engineering Department for his assistance in substrate surface preparation and scanning electron microscopy imaging. This research was funded by the U.S. Department of Energy under contract number DE-AC07-05ID14517.

Page intentionally left blank

CONTENTS

FIGURES

TABLES

ACRONYMS

AJP	aerosol jet printing
AM	advanced manufacturing
ASTM	American Society for Testing and Materials
DW	direct-write
INL	Idaho National Laboratory

Page intentionally left blank

Laser-based Adhesion Strength Measurements for Advanced Manufactured Sensor Adhesion Characterization

1. INTRODUCTION

Advanced manufacturing (AM) has emerged as the predominant enabler for innovation and design as it significantly expands the design envelope in terms of materials, form, and functionality. Additionally, AM technologies enable rapid prototyping, reduced production cost, and reduced material waste in comparison to classical fabrication methods [1]. Additive manufacturing technologies based on direct-write (DW) techniques, such as aerosol jet printing (AJP), Plasma Jet Printing, ink-jet printing, micro-dispense printing, and fused deposition modeling, have enabled the fabrication of components with complex geometries at the microscale (with features down to length scales of 10–25 μm), and have significantly reduced the concept-to-product development time [2]. Traditional approaches for fabricating complex and miniaturized sensors and devices, such as integrated circuits on semiconductor chips, rely on sophisticated and highly-precise tools such as ultraviolet photolithography, wet/dry reactive ion etching, and chemical vapor deposition, and require access to state-of-the-art cleanroom facilities. This requirement is often a barrier-to-entry for smaller research institutions that may not have their own cleanroom facility or the budget for access to pay-to-use cleanroom services [2]. Furthermore, the flexibility of device fabrication in cleanroom settings is severely reduced due to stringent contamination control requirements [3] and the production costs associated with changes to established processes [4]. Although still at its infancy, DW-based advanced manufacturing (AM) has shown potential in overcoming technical and economic barriers for prototyping and fabricating sensors and devices such as microelectromechanical systems at a large scale on a roll-to-roll basis [2].

Although research efforts over the past 2 decades have explored the application of DW techniques for manufacturing sensors and electronics for applications in wireless communications, electrochemical power devices, chemical and biological sensors, fuel cells, and flexible electronic displays [5], recent studies have opened the domain of DW technologies towards the development of novel in-pile sensors aimed at providing vital information needed for qualification of next-generation nuclear fuels and structural materials [6-8]. As part of the AM focus of the Department of Energy's Nuclear Energy Enabling Technologies Advanced Sensors and Instrumentation Program, new in-house capabilities to fabricate and test novel active and passive in-pile sensors are being developed at Idaho National Laboratory (INL). The program aims at developing and testing sensors manufactured using DW techniques for in-pile applications that can provide real-time, accurate, spatially resolved information regarding test conditions and the performance of fuels and materials during irradiation in a nuclear test reactor. Such sensors could be passive, such as peak temperature melt wires [6], or active, such as strain gauges or displacement transducers [7]. A prerequisite for such novel in-pile sensors is that they must be able to withstand the harsh environments of extreme temperature and irradiation conditions typically experienced in the core of a nuclear test reactor. Utilizing additive manufacturing techniques for sensor fabrication requires a substrate to serve as the surface that the print is mounted upon, and the application of printed devices is highly dependent upon the substrate used. With that, the interaction between the printed material and substrate is significant as it influences both print quality and device integrity. Therefore, determining optimal print process parameters associated with DW techniques needed for strong adhesion between the printed sensor and substrate is essential for meeting this prerequisite. Several studies have investigated the effect of substrate surface treatment on the adhesion of thin film sensors printed using DW techniques, such as AJP [9-13]. In most of these studies, the printed sensor-substrate adhesion was measured using Scotch™ tape peel tests (American Society for Testing and Materials [ASTM] D3359-09) [14] standardized by ASTM. Although the Scotch™ tape peel test has been widely adopted for testing the adhesion of thin films and coatings on substrates, there are limitations associated with this technique [15]. For instance, the adhesive strength measured using the peel test is often dependent on the type of tape used and the pressure applied on the printed film that can vary from user to

user. Furthermore, the peel test is destructive in nature and usually involves removal of centimeter-sized printed regions. Laser-based techniques, such as laser-induced spallation [16], and laser ablation [17–18], have been applied to the study of thin film adhesion. These techniques are non-contact and locally destructive (the damage region is limited to <200-μm-diameter spot) and are generally more repeatable when compared to the tape peel test. Therefore, laser-based methods show promise in evaluating the durability and robustness of in-pile sensors manufactured using AM/DW techniques.

This study reports the use of an all-optical, non-contact laser ablation technique to measure the sensor-substrate adhesion strength and determine the dominant combination of surface conditions and print process parameters that affect this interfacial adhesion. Sensors were printed using AJP and involved depositing silver nanoparticle inks on austenitic stainless steel 316L substrates. The substrate surface roughness was varied by polishing to different degrees of flatness, while the substrate surface energy was varied by treating the surface with oxygen plasma for varying durations. The effect of ink sintering conditions was also investigated by varying the ink sintering temperature and the ink sintering duration. Besides adhesion strength measurements, the influence of surface conditions and print process parameters on the sensor topography was also evaluated from measurements of the topography of the print using optical profilometry. The sensor-substrate interfacial adhesion strength was determined from the critical laser pulse energy required to ablate/detach the printed sensor from the substrate. Measurements of the sensor topography using optical profilometry revealed that post-deposition sintering at 400°C for 60 minutes resulted in a reduced sensor thickness, while plasma treating the substrate prior to printing yielded sensors with uniform thickness profiles transverse to the print direction. Sintering temperature and time were found to be the dominant parameters that affected sensor-substrate adhesion, followed by substrate surface roughness. The laser-based and locally destructive approach for adhesion strength measurements shows promise in overcoming the challenges and limitations of current standardized peel tests and can be developed into a post-fabrication process control protocol for evaluating the durability of AM-printed sensors in a high-throughput fashion. This work also lays the foundation for future studies aimed at using laser-induced spallation techniques as well as non-destructive laser ultrasonic methods for sensor-substrate adhesion characterization on sensors manufactured using AJP and other AM techniques, such as plasma jet printing.

2. EXPERIMENTAL METHODS AND MATERIALS

2.1 Substrate Surface Preparation

Austenitic stainless steel 316L plates with a thickness of 2.54 mm were acquired from OnlineMetals and were cut into 4 × 4 in. squares using a band saw. A total of 36 plates were cut for this study. The surface roughness of the stainless steel plates was altered by polishing using either 600-grit silicon carbide sandpaper, 800-grit silicon carbide sandpaper, or with a 1-μm diamond slurry. Of the 36 stainless steel plates, 12 were polished with the 600 grit sandpaper to achieve high-surface roughness, another 12 were polished with the 800-grid sandpaper for an intermediate surface roughness, and the final 12 plates were polished with the diamond paste for a mirror-like surface finish and low surface roughness. Figure 1 shows photographs of the stainless steel plates with high, intermediate, and low surface roughness, respectively. The average surface roughness in the three cases was measured in a representative 500 μm × 500 μm area of the stainless steel plate using a Veeco Wyko NT9100 optical profilometer in phase shifting interferometry mode. Figure 2 illustrates optical profilometry scans of the surfaces of the bare stainless steel substrates representing each of the three surface roughness cases. The average surface roughness in the stainless steel substrates representing the high, intermediate, and low roughness cases was determined to be 73.74 nm, 7.62 nm, and 2.72 nm, respectively. The black pixels in the profilometer scan for the high surface roughness substrate represent regions where reliable data points could not be acquired.

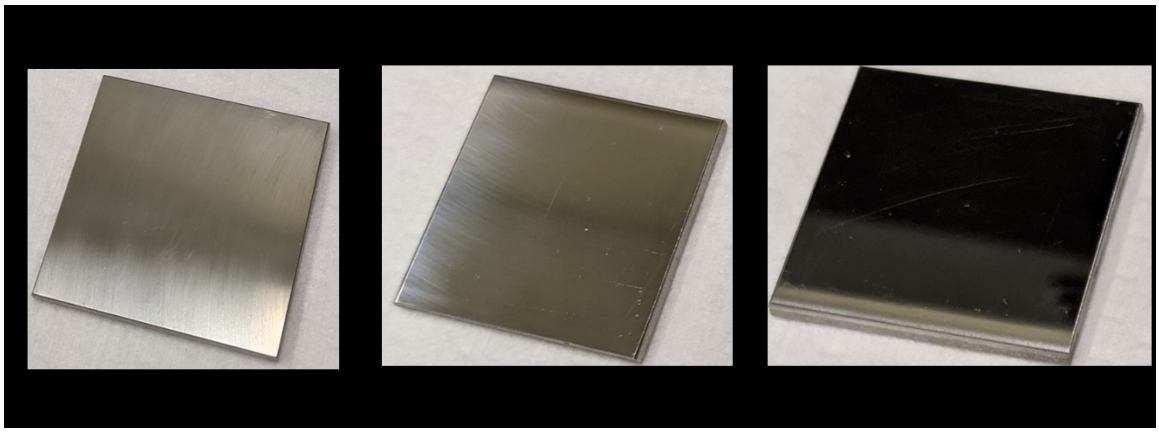

Figure 1. Stainless Steel 316L plates used as substrates in this study whose surface roughness was modified by polishing to different levels of surface finish.

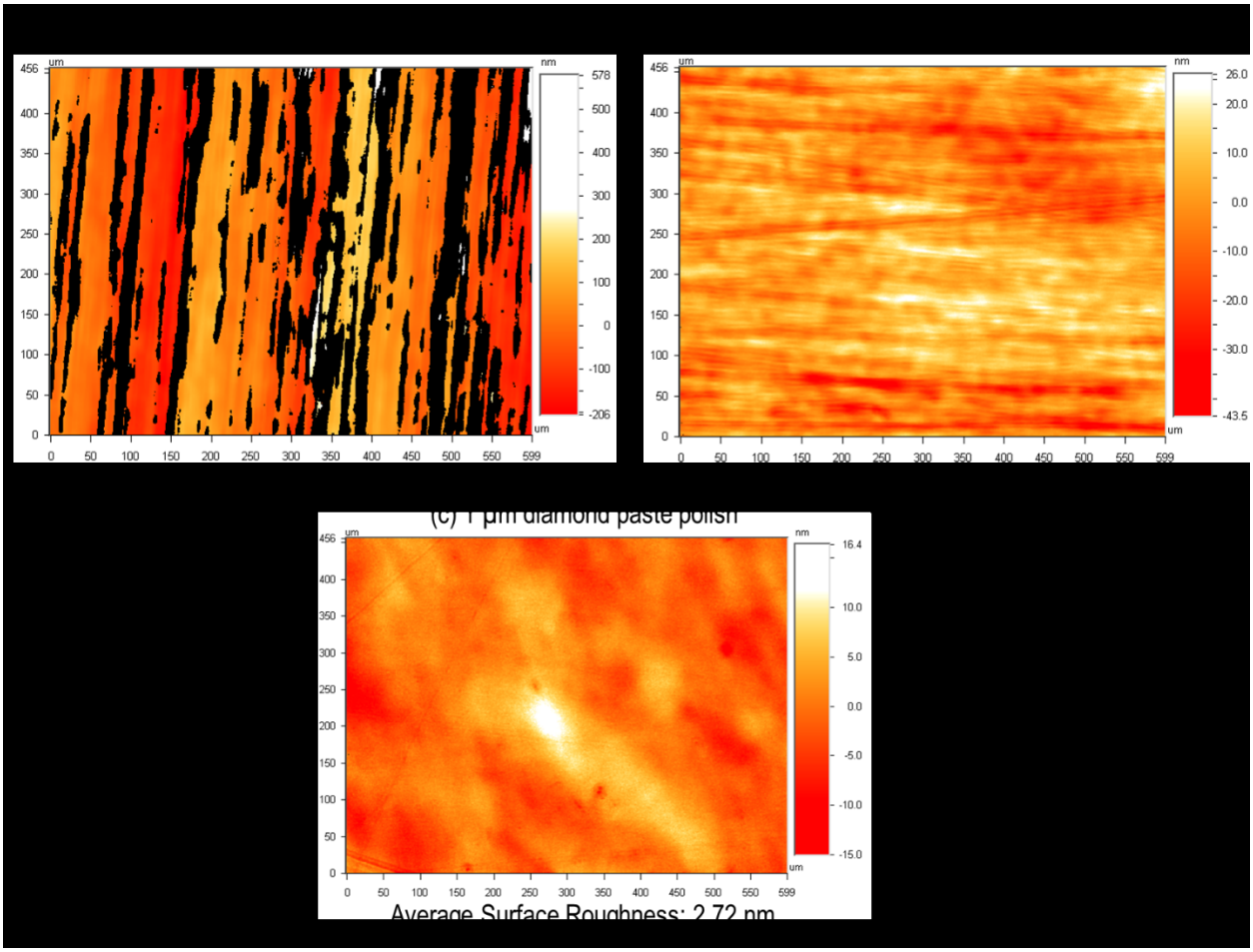

Figure 2. Optical profilometer scans in phase shifting interferometry mode used to determine the average surface roughness in a 500 µm × 500 µm region of the stainless steel plates polished to (a) high surface roughness; (b) intermediate surface roughness; and (c) low surface roughness.

2.2 Sensor Fabrication using Aerosol Jet Printing

Following the surface preparation of the stainless steel substrates, the sensors were then printed on the plates using an Optomec 200 AJP system located at Boise State University. A commercially available silver nanoparticle ink was used for the print. The ink comprised of silver nanoparticles dispersed in an organic solvent. The nanoparticle size distribution varied between ~100 and 200 nm in diameter. Prior to ink deposition, one-third of the 36 substrates were plasma treated using oxygen plasma for 5 minutes, another one-third were plasma treated for 2.5 minutes, while the final one-third batch of substrates was not given any plasma treatment. Plasma treatment is expected to alter the surface energy of the substrate, which in turn affects the contact angle of the ink droplet and ultimately, the adhesion of the deposited ink on the substrate. Ink deposition using AJP followed immediately after plasma treatment of the substrates. Three square sensor pads, with dimensions of 5 mm × 5 mm each, were printed on each of the 36 substrates. The width of each printed line pass was measured from optical micrographs and was found to vary between ~35 µm to ~55 µm. Following the ink deposition, the printed sensors were sintered in a furnace at either 250°C or at 400°C, for either 30 minutes or 60 minutes. Figure 3(a) shows an optical micrograph of a set of three printed sensor pads. A close-up view is shown in Figure 3(b).

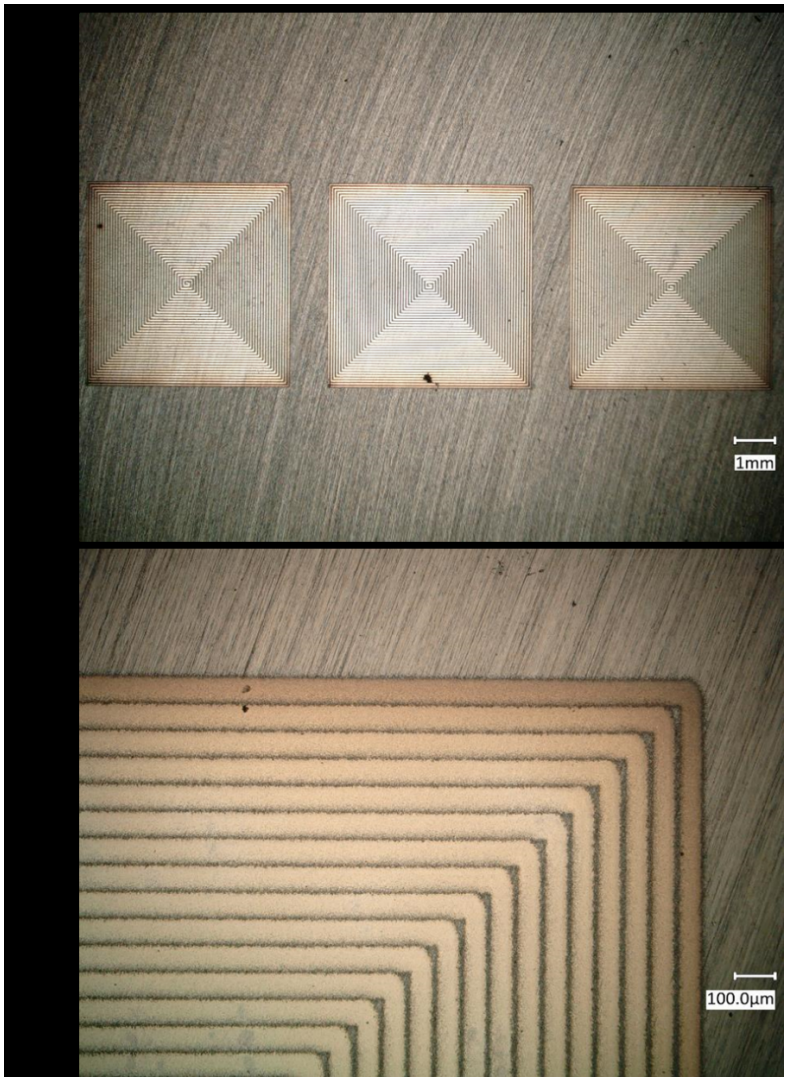

Figure 3. (a) Optical micrograph of three sensor pads printed using AJP; and (b) close-up view of the sensor pad.

Figure 4 shows a plot of the representative distribution of the measured widths of the printed lines along the vertical and horizontal orientations in one of the samples. The variation between ~35 µm to ~55 µm may be attributed to a slight eccentricity in the shape of the AJP nozzle (i.e., not being perfectly circular). This variation was seen in most of the samples and was not attributed to a substrate surface or print process parameter.

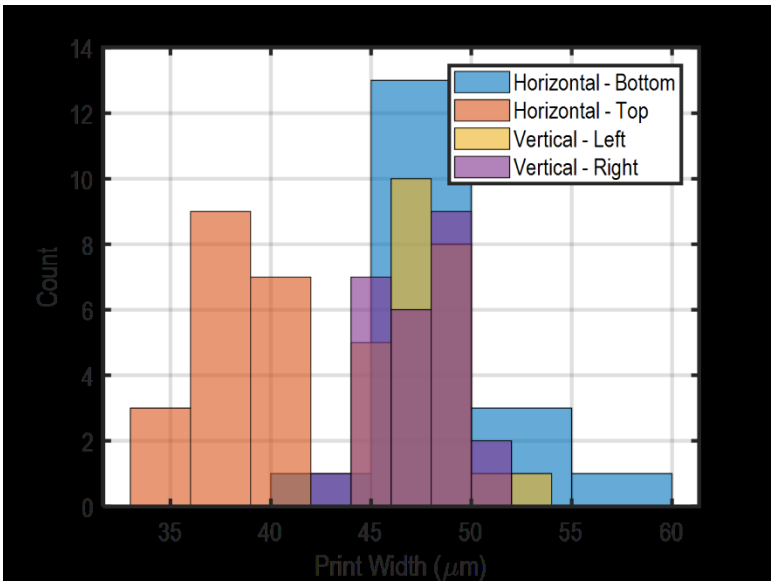

Figure 4. Distribution of the print widths along the horizontal and vertical orientations measured from the optical micrographs.

The substrate surface conditions (surface roughness and surface energy) as well as ink treatment conditions (sintering temperature and duration) were varied in a systematic approach (known as a factorial design of experiment) so that each of the 36 samples had a unique combination of substrate/ink treatment parameter levels. The 36 samples were divided into six groups, wherein samples in each group had a fixed plasma treatment time and sintering temperature. The sample test matrix resulting from the factorial design of experiment that lists the print conditions for each of the 36 substrates is listed in Table 1.

Table 1. Sample test matrix listing each of the substrate surface and ink treatment parameters that were varied in a factorial design of experiment approach.

Sample ID	Group	Plasma Time (minutes)	Sinter Temperature (°C)	Sinter Time (minutes)	Surface Roughness
001	1	5	250	30	Low
002		5	250	30	Intermediate
003		5	250	30	High
004		5	250	60	Low
005		5	250	60	Intermediate
006		5	250	60	High
007	2	5	400	30	Low
008		5	400	30	Intermediate
009		5	400	30	High
010		5	400	60	Low
011		5	400	60	Intermediate
012		5	400	60	High
013	3	2.5	250	30	Low
014		2.5	250	30	Intermediate
015		2.5	250	30	High
016		2.5	250	60	Low
017		2.5	250	60	Intermediate
018		2.5	250	60	High
019	4	2.5	400	30	Low
020		2.5	400	30	Intermediate
021		2.5	400	30	High
022		2.5	400	60	Low
023		2.5	400	60	Intermediate
024		2.5	400	60	High
025	5	0	250	30	Low
026		0	250	30	Intermediate
027		0	250	30	High
028		0	250	60	Low
029		0	250	60	Intermediate
030		0	250	60	High
031	6	0	400	30	Low
032		0	400	30	Intermediate
033		0	400	30	High
034		0	400	60	Low
035		0	400	60	Intermediate
036		0	400	60	High

2.3 Sensor Topography Measurements

The effect of substrate surface conditions (roughness and surface energy) and post-deposition ink treatment (sintering temperature and duration) on the printed sensor thickness was determined by optical profilometry measurements using a Veeco Wyko NT9100 optical profilometer in vertical scanning interferometry mode. Measurements were made in a 50 μm × 50 μm region that spanned ~5 printed lines by imaging the sample surface with a 50× microscope objective lens. Sensor thickness profiles along the print direction and transverse to the print direction were analyzed.

2.4 Adhesion Measurements using Laser Ablation

The interfacial adhesion strength between the printed sensor and the stainless steel substrate was determined by employing a laser ablation technique using facilities available in the Laser-based Materials Characterization Laboratory located at the INL Research Center. A 532-nm pulsed diode-pumped solid-state laser (TEEM Photonics) with a pulse duration of 440 ps, pulse repetition rate of 1 kHz, and a maximum pulse energy of 14 μJ was used for the laser ablation measurements. The laser beam had a Gaussian intensity distribution along the radial direction and was focused on the surface of the sample directly on the printed sensor to a spot of ~200 μm in diameter. The sensor was irradiated with the laser beam for ~5 seconds, which corresponded to irradiation with ~5000 laser pulses. The laser pulse energy was adjusted by rotating a half wave plate used in conjunction with a polarizing beam splitter cube and was progressively increased until the threshold of detachment/ablation of the printed sensor from the substrate was observed. The relative adhesion strength was determined from the critical laser pulse energy required for the onset of ablative damage/ejection of sensor from the substrate. The damaged region was confined to a ~200-μm spot on the surface of the sample. Figure 5 shows an optical micrograph of a laser-ablated damage region on Sample 001 created by irradiation with 4-μJ laser pulses. The bare substrate is seen in the center of the irradiated spot due to removal of the sensor material in that region. The dark ring around the ejected region is likely due to oxidation of the silver following rapid heating due to absorption of the laser pulse energy.

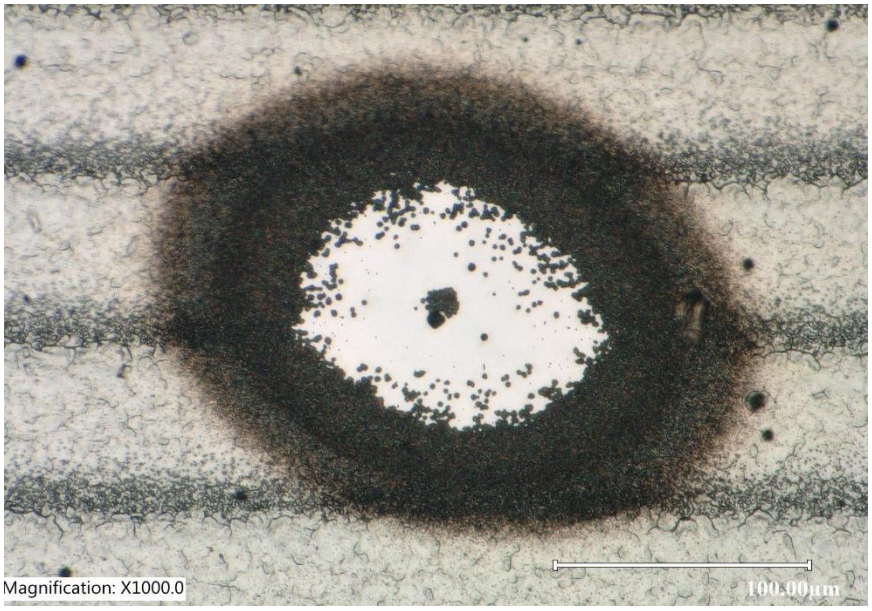

Figure 5. Removal of the printed sensor region in the center of a spot irradiated with laser pulses with energy of 4 μJ.

3. RESULTS AND DISCUSSION

3.1 Silver Nanoparticle Ink Sintering

High-magnification images of the printed sensors were acquired using scanning electron microscopy on a few samples to ascertain the level of sintering of the silver nanoparticle ink for different furnace temperature (250°C or 400°C), or for short (30 minutes) or long durations (60 minutes). Figure 6 shows a comparison of a silver nanoparticle ink that was sintered at 250°C for 30 minutes (in Sample 001), and at 400°C for 60 minutes (in Sample 036). Qualitatively, the scanning electron microscopy images show that in both cases, the silver nanoparticles are well sintered and appear as a continuous coagulated thin film. Some individual nanoparticles that were sprayed on either side of the line width were observed.

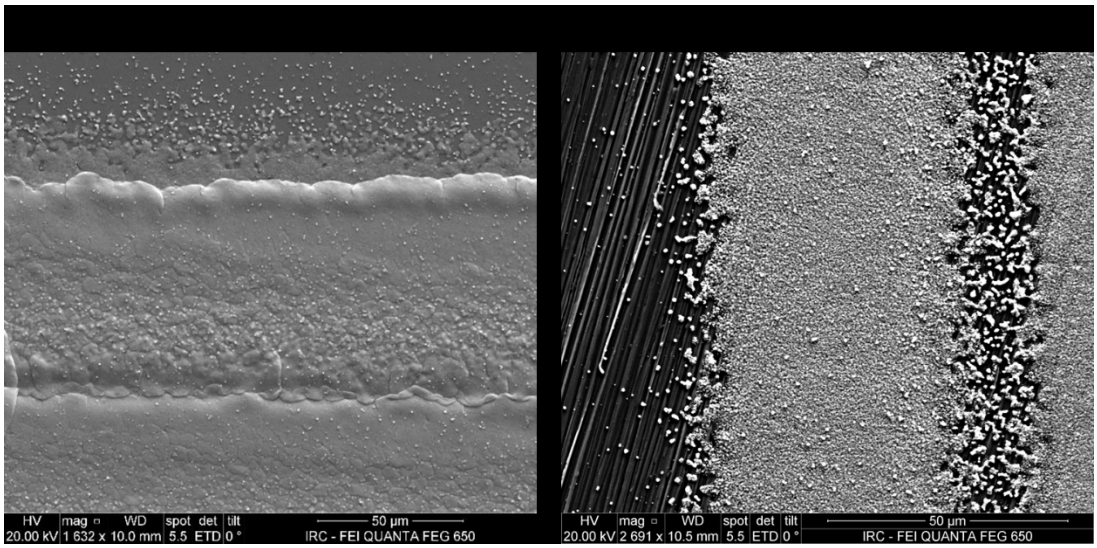

Figure 6. Scanning electron microscopy images showing details of the silver nanoparticle sintering level in Sample 001 and Sample 036.

Previous studies have investigated the sintering and coalescence of silver nanoparticles and found that the nanoparticles sintered into continuous films at temperatures as low as 200°C [19]. The sintering at 200°C, although much below the melting point of bulk silver (960°C), is usually attributed to the reduced melting point of the nanoparticles compared to that of bulk metal and to the surface pre-melting [19].

3.2 Sensor Topography Characterization

Optical profilometer scans were used to analyze the effect of substrate surface conditions (surface roughness and surface energy) and ink treatment conditions (sintering temperature and sintering time) on the thickness profile along the print direction, and transverse to the print direction. In general, the sensor thickness was uniform along the print direction and varied between 0.5 µm to 2.0 µm transverse to the print direction. Plasma treatment was found to be the dominant factor that affected the thickness profile of the print transverse to the print direction. In most cases, plasma treatment yielded uniform thickness profiles, while in samples that were not plasma treated (or plasma treated for shorter durations), the thickness at the edges of a single pass print was higher, with a “dip” in the central region of the print due to reduced thickness. The non-uniform thickness of the print in the transverse direction in samples that were not plasma treated or plasma treater for short durations may be attributed to the higher contact angle of the ink droplet on the substrate in these samples. This is expected to pull the silver nanoparticles to the meniscus along the droplet drying front, resulting in higher material deposition along the edges of the print. The contact angle on the plasma treated substrates is expected to be much lower due to the droplet spreading to a thin film, resulting in uniform nanoparticle deposition along the width of the print. The effect of the contact angle and droplet evaporation rate on the morphology of inkjet-printed lines was

thoroughly investigated by Soltman and Subramanian [20]. Their results showed a similar increase in thickness at the edges of the print under certain conditions and this was attributed to the "coffee ring" effect (i.e., the effect of contact angle wherein the ink particles are transferred to the droplet rim).

Figure 7 shows the optical profilometer scans of two lines in samples from Group 2 (i.e., samples that were plasma treated for 5 minutes, and sintered at 400°C). Samples 007, 008, and 009 were sintered at 400°C for 30 minutes, while samples 010, 011, and 012 were sintered at 400°C for 60 minutes. The thickness of the print in the 30-minute sintered samples was ~2 µm at the edges of the print and varied between 1.0 and 1.5 µm in the center of the print. The samples that were sintered for 60 minutes, on the other hand, had a consistent thickness of ~1.5 µm.

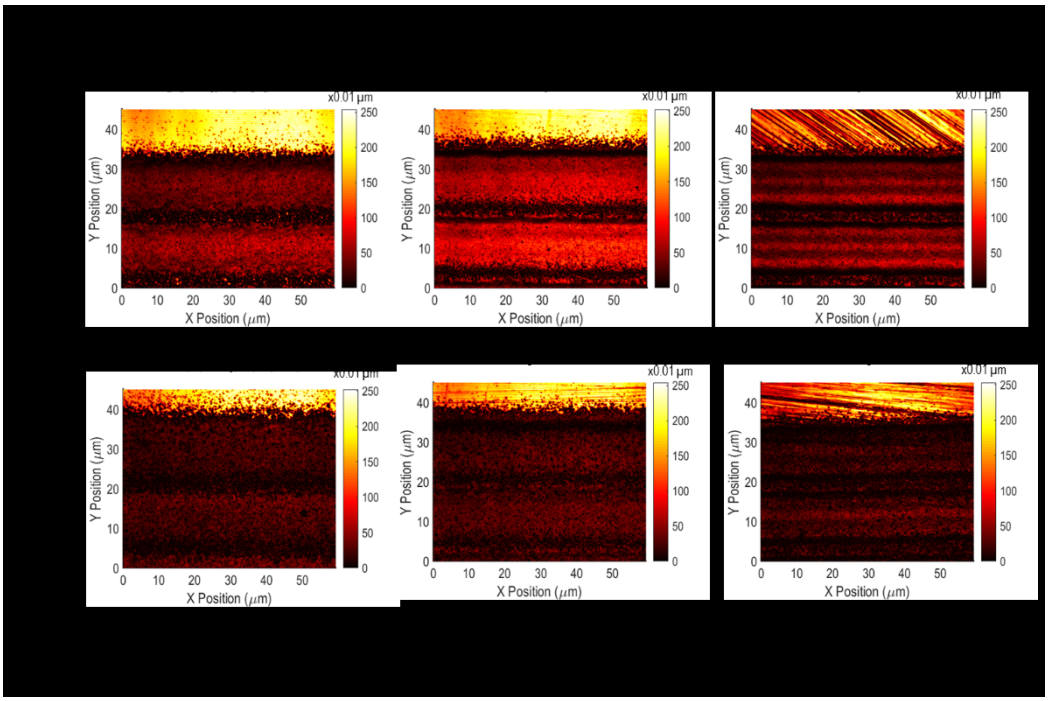

Figure 7. Optical profilometer scans of samples from Group 2.

The thickness profiles along the orthogonal to the print direction for samples from Group 2 are shown in Figure 8. The measurements indicate that although plasma treatment is an important parameter for attaining uniform print thickness, the sintering duration also affects the thickness profile. In this case, the 60-minute sintered samples exhibited a reduced dip in the center of the print, suggesting that this may be the preferred duration for the ink to flow and the nanoparticles could coalesce into a uniform thickness.

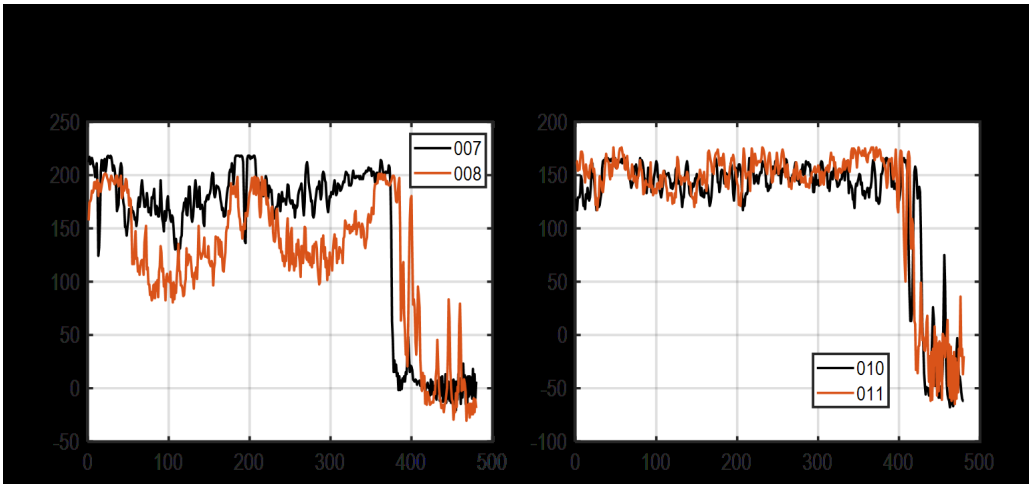

Figure 8. Thickness profiles in Group 2 samples sintered for 30 and 60 minutes at 400°C and plasma treated for 5 minutes.

Profilometer scans on the samples whose substrates were not plasma treated prior to ink deposition, or were plasma treated for only 2.5 minutes showed greater variations in the thickness profiles. The thickness of the print was clearly higher at the edges of the print, with noticeable dips in the center, as seen in Figure 9.

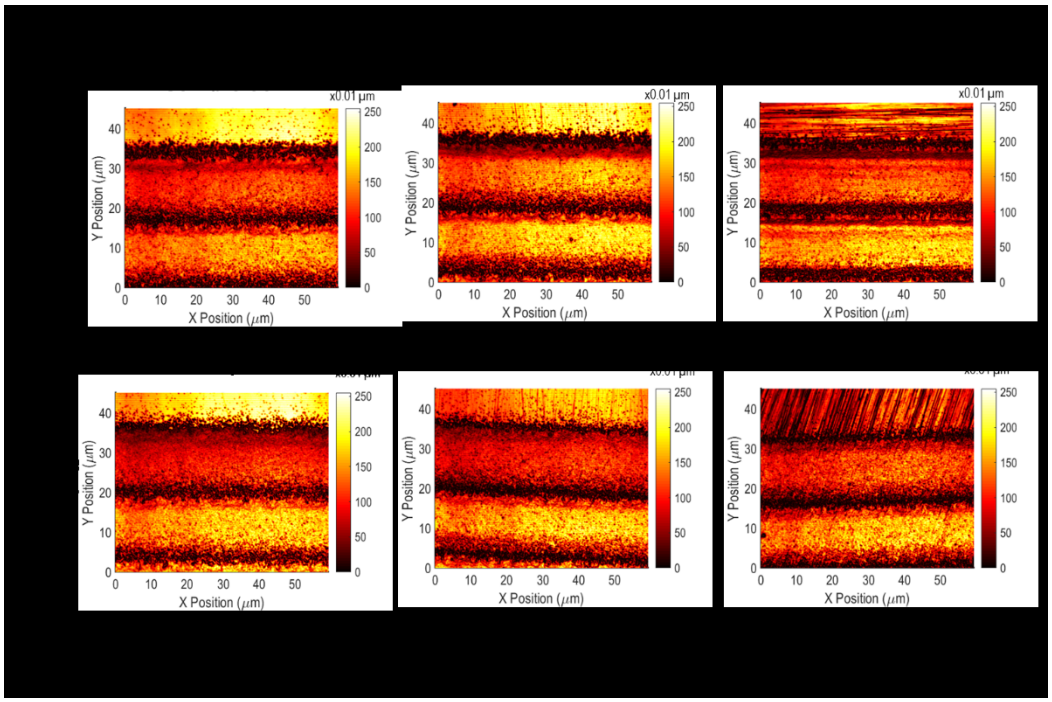

Figure 9. Optical profilometer scans of samples from Group 6.

Thickness profiles for select samples from Group 6 are illustrated in the plots in Figure 10. The thickness at the edges of the print was found to be ~2 µm, while that at the center was considerably lower, ranging from 0.3 to 1 µm. This observation highlights the drastic effect of the substrate surface energy and plasma treatment on the morphology of the sensor. A similar analysis of samples from other groups confirmed that plasma treatment yielded uniform thickness across a single print. The depth of the dip in the center of the print was found to grow larger when going from a 5-minute plasma-treated sample, to a

2.5-minute plasma-treated sample, to finally no plasma treatment. Sintering time and duration were also found to be secondary factors that affected the thickness profile of the printed sensor. Sintering at 400°C for 60 minutes yielded consistently thinner films when compared to sintering at 400°C for 30 minutes, or at 250°C for 30 or 60 minutes. Optical profilometer scans from samples in all groups are shown in Appendix A of this report.

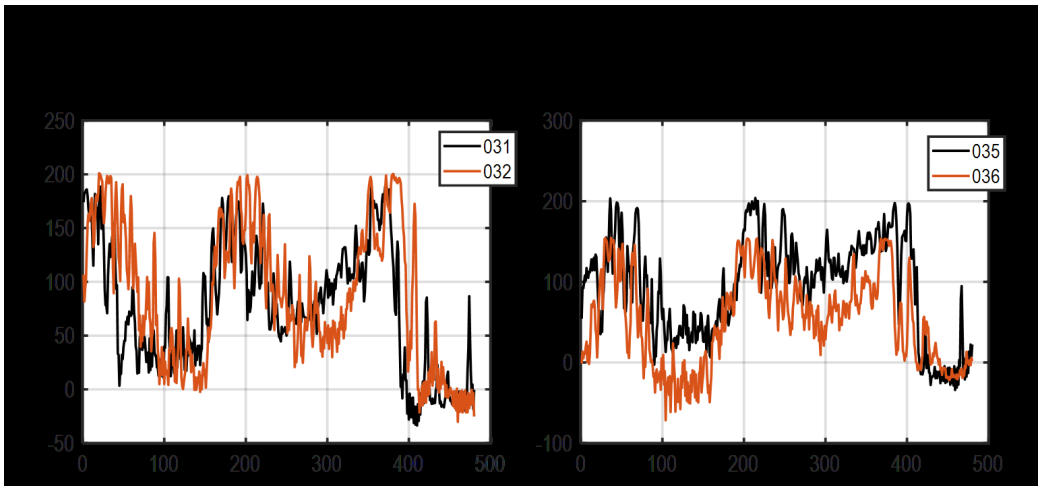

Figure 10. Thickness profiles in Group 6 samples sintered for 30 and 60 minutes at 400°C with no substrate plasma treatment.

Besides the sensor topography (in terms of the thickness profiles of the prints), the appearance/color of the silver sensor pads was also affected by sintering temperature and duration. Figure 11 shows images of Sample 005 (from Group 1), and Sample 010 (from Group 2). Sample 005 was sintered at 250°C for 60 minutes, while Sample 010 was sintered at 400°C also for 60 minutes. The sensor pads in samples that were sintered at 400°C for either 30 or 60 minutes were found to have a darker appearance when compared to samples that were sintered at 250°C for either 30 or 60 minutes. Since the samples were sintered in a furnace with an air environment, the darker appearance of the high-temperature sintered samples may be attributed to the formation of an oxide layer on the sensor pads. Further analysis using energy-dispersive X-ray spectroscopy could be used to understand differences in the elemental composition of the printed sensors in samples that were sintered at 250°C and those that were sintered at 400°C. The effect of this possible oxidation on the performance of the sensor (in terms of electrical resistivity, and other physical properties) should also be investigated in the future studies.

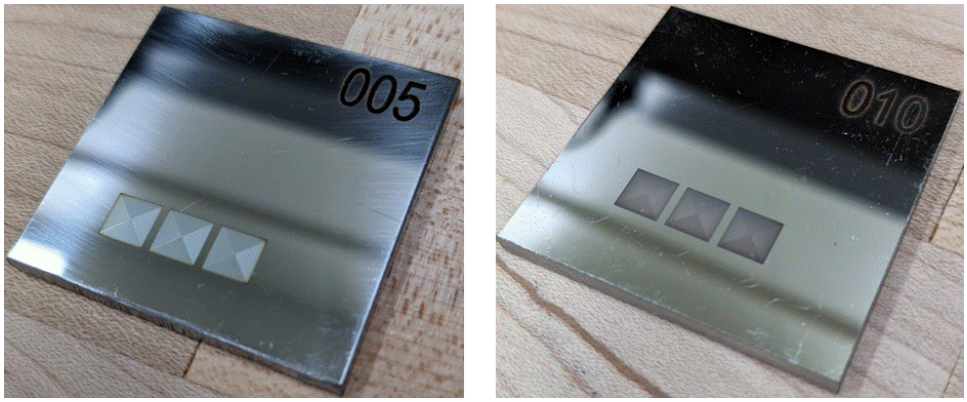

Figure 11. Photographs of samples that were sintered at 250°C (Sample 005) and at 400°C. The darker appearance of the sensor pad in samples that were sintered at 400°C could be attributed to an oxide layer formation on the silver films.

3.3 Sensor-Substrate Adhesion Measurements using Laser Ablation

The results from the laser ablation tests on the complete test matrix of 36 samples for determining the threshold laser pulse energy required for ejection/removal of the sensor from the substrate via thermoelastic or ablative mechanisms are summarized in Figure 12.

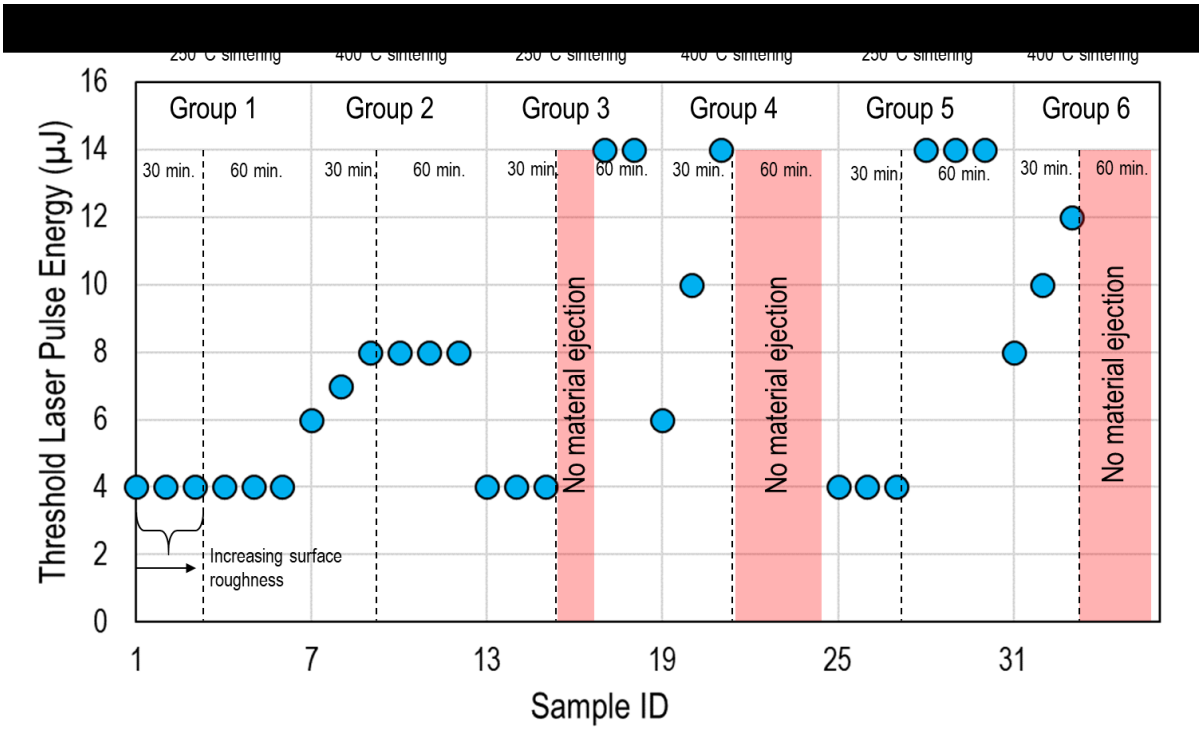

Figure 12. Summary of the measured threshold laser pulse energy for all 36 samples required for sensor detachment from the substrate that was used as a measure of the interfacial sensor-substrate adhesive strength. Each set of three consecutive data points represent substrates with increasing surface roughness.

All samples from Group 1 (whose substrates were plasma treated for 5 minutes and whose ink was sintered at 250°C for either 30 or 60 minutes) exhibited a threshold laser pulse energy of 4 µJ required for sensor detachment. This was regardless of substrate surface roughness. The sensor detachment occurred either in the center of the excited region (as seen in Figure 5), or predominantly at the edge of the print (as see in Figure 13). The dark circular region around the ejected sensor location is most likely localized oxidation due to rapid heating by the laser pulses. A lighter ring was seen in Samples 001–003 (all of which were sintered for 30 minutes), while this ring was not seen in Samples 004–006 (all of which were sintered for 60 minutes). This "ring"-like feature could represent a lower oxidation level due to reduced laser intensity near the periphery of the laser beam. The absence of this ring-like feature suggests that the samples sintered for 60 minutes may already have a thin oxide layer on the sensor; therefore, there may be minimal further oxidation at the periphery of the laser irradiated region. However, in all cases no distinct effect of surface roughness or sintering duration on the sensor-substrate was observed.

In Group 2 (where sample substrates were plasma treated for 5 minutes and whose ink was sintered at 400°C for either 30 or 60 minutes), the threshold laser pulse energy required for sensor detachment varied between 6 µJ to 8 µJ. The first half of samples in Group 2 (Samples 007, 008, and 009) were all sintered at 400°C for 30 minutes. These samples exhibited a clear dependence of the substrate surface roughness on the sensor-substrate adhesion, with the sample with the smooth substrate having a threshold detachment energy of 6 µJ, the sample with the intermediate roughness having a 7-µJ threshold energy, and the sample with the rough substrate having a threshold energy of 8 µJ. Substrates with higher surface roughness are expected to yield a higher sensor-substrate adhesion strength, since the effective contact

surface area between the sensor and substrate is expected to be higher. However, a similar dependence of the adhesive strength on the surface roughness was not seen in the samples sintered at 400°C for 60 minutes. This suggests that the ink has coagulated to a continuous film to a greater extent in the samples that were sintered for 60 minutes, thereby reducing the influence of the geometrical aspect of mechanical contact between the sensor and substrate.

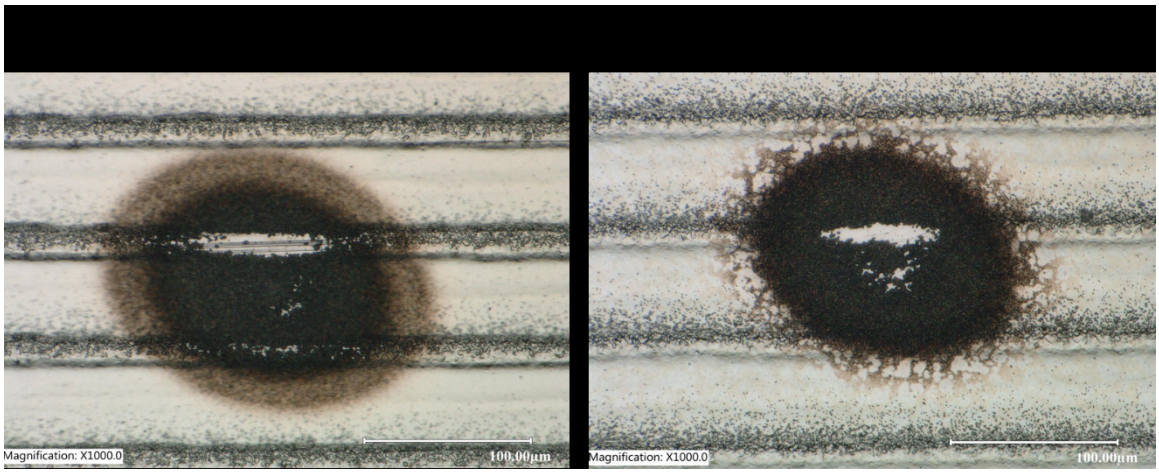

Figure 13. Optical micrographs showing laser-ablated regions from two samples in Group 1. Sample 003 was sintered at 250°C for 30 minutes, while Sample 005 was sintered at the same temperature for 60 minutes. The lighter secondary ring-like feature around the periphery of the irradiated spot was only seen in the 30-minute sintered samples.

The first half of Group 3 samples all exhibited a threshold laser pulse energy of 4 µJ, similar to Group 1 samples. Like the samples in Group 1, these Group 3 samples were also sintered at 250°C for 30 minutes. The only difference between the Group 1 and Group 3 samples was the plasma treatment duration (Group 1 samples were plasma treated for 5 minutes, while Group 2 were plasma treated for 2.5 minutes). The failure mode in the first half of Group 3 samples was also similar to that seen in Group 1 samples, with the predominant failure of the sensor occurring in the center of the irradiated spot. Samples in the second half of Group 3 all had a higher threshold laser pulse energy required for sensor ejection. Sample 016 did not exhibit sensor detachment even at the highest laser pulse energy of 14 µJ. The printed sensors in samples 017 and 018, on the other hand, were found to detach at the maximum pulse energy of 14 µJ, predominantly at the edges of the print. While the first half of the sample set in Group 3 had the characteristic oxidation marks in the laser-irradiated region (shown in the left pane of Figure 14), the dark laser-induced oxidation marks were not observed in samples in the latter half of Group 3 (right pane of Figure 14). Instead, the irradiated region appeared slightly brighter.

Like in the case of Group 2, the sensor-substrate adhesion strength in the samples in Group 3 exhibited a strong dependence on the sintering duration. When compared to samples in Group 2 that were sintered at 400°C; however, the samples in Group 3 were sintered at 250°C. Despite the lower sintering temperature, the Group 3 samples exhibited a considerably higher threshold laser pulse energy needed for sensor ejection. This may be attributed to the effect of plasma treatment of the substrate surface. The samples in Group 2 were plasma treated for 5 minutes, while those in Group 3 were plasma treated for 2.5 minutes. Although plasma treatment is expected to activate the substrate surface and increase the surface energy needed for improved sensor-substrate interfacial adhesion, the laser ablation measurements indicate that beyond a critical duration of plasma treatment, the surface energy may be altered to reduce sensor-substrate adhesion. The effect of plasma treatment duration on the surface energy of stainless steel 316L has been investigated previously [21]. Williams et al.'s 2017 article found an optimal duration of 15 seconds of treating the 316 stainless steel plates with cold atmospheric plasma that led to a reduction in carbon contamination [21]. Measurements in this study suggest that the substrates treated with oxygen plasma for 2.5 minutes are well-suited for strong sensor-substrate adhesion, and plasma treating the

substrates for longer results in a detrimental effect on the sensor-substrate adhesion.

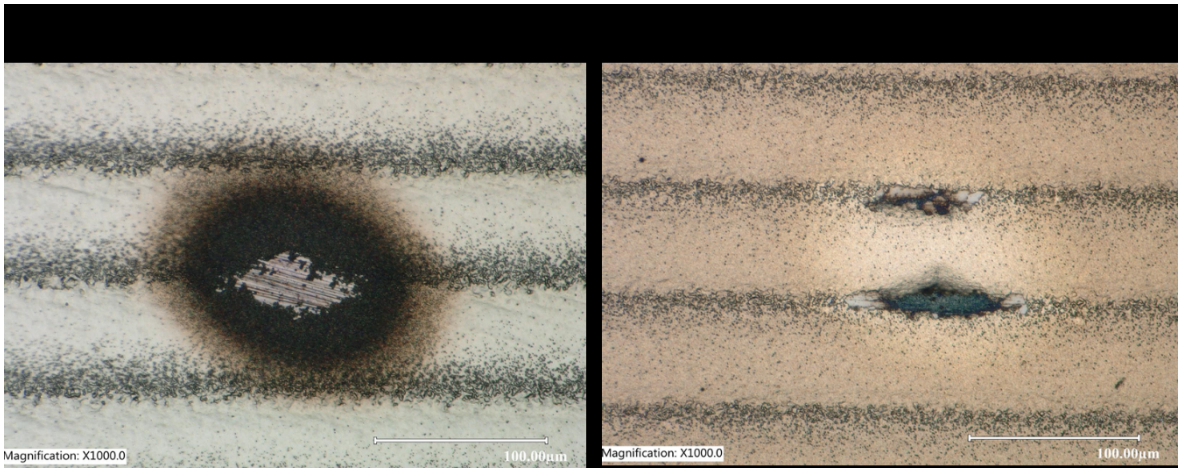

Figure 14. Optical micrographs of samples in Group 3 highlighting representative laser-induced damage in samples in the first half (left) and latter half (right) of Group 3.

Samples in Group 4 were all plasma treated for 2.5 minutes, and sintered at 400°C. The first half of the samples in Group 4, all of which were sintered for 30 minutes, exhibited a dependence of surface roughness on the sensor-substrate adhesion energy, like in the case of the samples in the first half of Group 2 where the adhesion was the highest in the roughest substrate. The fact that the threshold laser pulse energy required for sensor ejection in the samples in the first half of Group 4 was almost twice the corresponding values for the samples in Group 2 again highlights the influence of plasma treatment duration (samples in Group 2 were plasma treated for 5 minutes, while those in Group 4 were treated with oxygen plasma for 2.5 minutes). The second half of samples in Group 4 that were sintered at 400°C for 60 minutes and plasma treated for 2.5 minutes did not show any visible laser-induced damage up to the maximum laser pulse energy of 14 µJ. The substrate surface treatment (2.5-minute oxygen plasma cleaning) and ink sintering conditions (400°C for 60 minutes) in this set of samples (Samples 022, 023, and 024) show that these conditions resulted in the most robust sensors. The effect of surface roughness was not seen in this set of samples (Samples 022, 023, and 024).

Samples in Groups 5 and 6 were not plasma treated, and instead, the inks were deposited using the AJP printer on the as-received substrate surfaces. The samples in Group 5 were sintered at 250°C, while those in Group 6 were sintered at 400°C. In the first half of the sample in Group 5, all of which were sintered at 250°C for 30 minutes, the critical threshold energy was very low, at 4 µJ, regardless of substrate surface roughness. However, the critical threshold energy for samples in the second half of Group 5 occurred at the highest laser pulse energy of 14 µJ. These samples were sintered at 250°C for 60 minutes. The effect of sintering duration is again clearly highlighted through the measurements on Group 5 samples. A similar effect of sintering duration was seen in the samples of Group 6. For samples in the first half of Group 6 (sintered for 30 minutes), the effect of surface roughness on the adhesion strength was observed. The Group 6 samples that were sintered for 60 minutes also were seen to be the most resilient—with no observable damage even after irradiating at the highest laser pulse energy of 14 µJ. This is similar to the case of samples in Group 4 and shows that when the silver nanoparticle inks are sintered at 400°C for 60 minutes, surface roughness or surface energy (due to plasma treatment) are not dominant parameters that dictate the sensor-substrate adhesion strength.

4. SUMMARY AND CONCLUSIONS

In summary, a laser-based ablation technique is used to systematically study the effect of substrate surface conditions and ink treatment parameters on the sensor-substrate adhesion strength of sensors printed onto austenitic stainless steel 316L substrates using AJP. The sensors comprised of silver nanoparticle inks that were printed using AJP by varying the substrate surface roughness, substrate

surface energy (using as-received substrates or by treating them with oxygen plasma for 2.5 or 5 minutes), the ink sintering temperature (250°C or 400°C), and the ink sintering duration (30 or 60 minutes). The locally destructive (limited to <200-µm-diameter circular regions on the sample), and all-optical, non-contact laser-based measurements of the sensor-substrate adhesion revealed that the sintering duration and sintering temperature were the two dominant factors that determined the quality and durability of the sensor-substrate interface. Samples that were sintered at 400°C for 60 minutes were found to be the most robust, with no laser-induced damage even at the maximum laser pulse energy of 14 µJ. The samples that were plasma treated for 5 minutes (and sintered at 400°C for 60 minutes) were the exception to this observation and had a threshold laser pulse energy for sensor detachment of ~8 µJ. The measurements indicate that plasma treating for longer than 2.5 minutes may be detrimental to sensor-substrate adhesion strength. In all cases, samples that were sintered for 60 minutes (whether at 250°C or at 400°C) exhibited superior sensor-substrate adhesion strength when compared to those that were sintered for 30 minutes. The substrate surface roughness was also found to be a secondary parameter that affected sensor-substrate adhesion strength, only in the cases of sensors that were sintered at 400°C for 30 minutes.

The experimental methodology presented in this study shows promise in evaluating environmental factors that influence the quality, robustness, and durability of sensors fabricated using AM DW techniques. Although locally destructive in nature, the non-contact aspect of our laser-based approach for thin film adhesion measurement has the potential to overcome the challenges of currently used ASTM standards based on peel tests. This approach is particularly promising for the development of novel in-pile sensors and could be used as a process control tool following fabrication, and right before deployment in a nuclear test reactor. Future studies will investigate other laser-based techniques, such as laser-induced spallation, and laser ultrasonics that are locally destructive or are completely non-destructive. These approaches will be used to evaluate the quality of new in-pile sensors printed using DW techniques, such as plasma jet printing, that could further our understanding of process parameters in AM and their influence of sensor performance and integrity.

5. REFERENCES

1. Goyal, S., and S. Grover. 2012. “Advanced manufacturing technology effectiveness: A review of literature and some issues.” *Frontiers of Mechanical Engineering* 7, no. 3: 256–267, https://doi.org/10.1007/s11465-012-0330-7.
2. Teh, K. S. 2017. “Additive direct-write microfabrication for MEMS: A review.” *Frontiers of Mechanical Engineering* 12, no. 4: 490–509, https://doi.org/10.1007/s11465-017-0484-4.
3. Osburn, C., H. Berger, R. Donovan, G. Jones. 1988. “The effects of contamination on semiconductor manufacturing yield,” *The Journal of Environmental Sciences* 31, no. 2: 45–57, https://doi.org/10.17764/jiet.1.31.2.9863780552351680.
4. Iwai, H., K. Kakushima, H. Wong, 2006. “Challenges for future semiconductor manufacturing,” *International Journal of high Speed Electronics and systems* 16, no.1: 43–81, https://doi.org/10.1142/9789812773081_0004.
5. Piqué, A., Chrisey, D. B. (Eds.). “Direct-write technologies for rapid prototyping applications: sensors, electronics, and integrated power sources,” *Elsevier*.
6. Mondal, K., K. Fujimoto, and M. D. McMurtrey. 2020. “Advanced Manufacturing of Printed Melt Wire Chips for Cheap, Compact Passive In-Pile Temperature Sensors.” *JOM* 72, no.12: 4196–4201.
7. Estrada, D., M. D. McMurtrey, and K. Fujimoto. 2018. In-Pile Instrumentation Advanced Manufacturing: Development of Pt, Mo, and Nb Inks. INL/EXT-18-52347-Rev000. Idaho National Laboratory, Idaho Falls, Idaho (United States).
8. Rempe, J., H. MacLean, R. Schley, D. Hurley, J. Daw, S. Taylor, J. Smith, J. Svoboda, D. Kotter, D. Knudson, S. C. Wilkins, M. Guers, L. Bond, L. Ott, J. McDuffee, E. Parma, and G. Rochau. 2011. *New In-pile Instrumentation to Support Fuel Cycle Research and Development.* INL/EXT-10-19149.

Idaho National Laboratory.

9. Vunnam, S., K. Ankireddy, J. Kellar, and W. Cross. 2013. “Surface modification of indium tin oxide for direct writing of silver nanoparticulate ink micropatterns.” *Thin Solid Films* 531: 294–301.
10. Wilkinson, N. J., M. A. A. Smith, R. W. Kay, and R. A. Harris, 2019. “A review of aerosol jet printing—a non-traditional hybrid process for micro-manufacturing.” *The International Journal of Advanced Manufacturing Technology* 105, no. 11: 4599–4619.
11. Mahajan, A., C. D. Frisbie, and L. F. Francis, 2013. “Optimization of aerosol jet printing for high-resolution, high-aspect ratio silver lines.” *ACS Applied Materials & Interfaces* 5, no. 11: 4856–4864.
12. Mette, A., P. L. Richter, M. Hörteis, and S. W. Glunz. 2007. “Metal aerosol jet printing for solar cell metallization.” *Progress in Photovoltaics: Research and Applications* 15, no. 7: 621–627.
13. Hung, K. Y., Y. T. Chang, C. H. Chien, C. F. Ding, M. C. Tsai, and H. T. Young. 2020. “Investigation of ink modification for aerosol jet printing process on FR-4 substrate.” *The International Journal of Advanced Manufacturing Technology* 111, no. 3: 1147–1156.
14. ASTM, S. 2009. “Standard test methods for measuring adhesion by tape test.” *Annu. B. ASTM Stand*. 6: 1–8.
15. Mittal, K. L. 1978. “Adhesion measurement: Recent progress, unsolved problems, and prospects.” *Adhesion measurement of thin films, thick films, and bulk coatings*: 5–17.
16. Wang, J., R. L. Weaver, and N. R. Sottos. 2002. “A parametric study of laser induced thin film spallation.” *Experimental Mechanics* 42, no. 1: 74–83.
17. Mittal, K. L., and W. S. Lei, (Eds.). 2018. *Laser Technology: Applications in Adhesion and Related Areas*. John Wiley & Sons.
18. Min, J., H. Wan, B. E. Carlson, J. Lin, and C. Sun, 2020. “Application of laser ablation in adhesive bonding of metallic materials: A review.” *Optics & Laser Technology* 128: 106188.
19. Magdassi, S., M. Grouchko, O. Berezin, and A. Kamyshny. 2010. “Triggering the sintering of silver nanoparticles at room temperature.” *ACS Nano* 4, no. 4: 1943–1948.
20. Soltman, D., and V. Subramanian. 2008. “Inkjet-printed line morphologies and temperature control of the coffee ring effect.” *Langmuir* 24, no. 5: 2224–2231.
21. Williams, D. F., E. J. Kellar, D. A. Jesson, and J. F. Watts. 2017. “Surface analysis of 316 stainless steel treated with cold atmospheric plasma.” *Applied Surface Science* 403: 240–247.

Appendix A

Optical Profilometer Scans on All Samples in Test Matrix

Appendix A

Optical Profilometer Scans on All Samples in Test Matrix

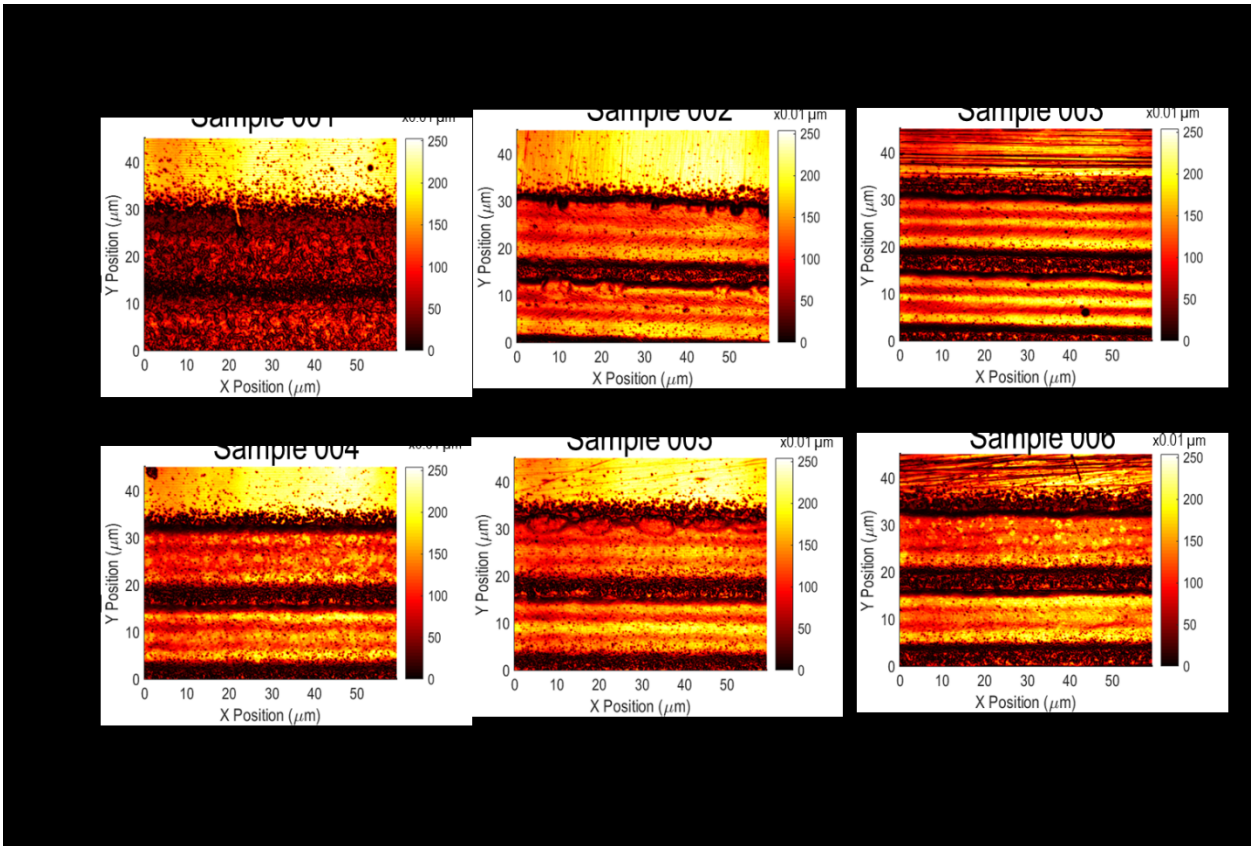

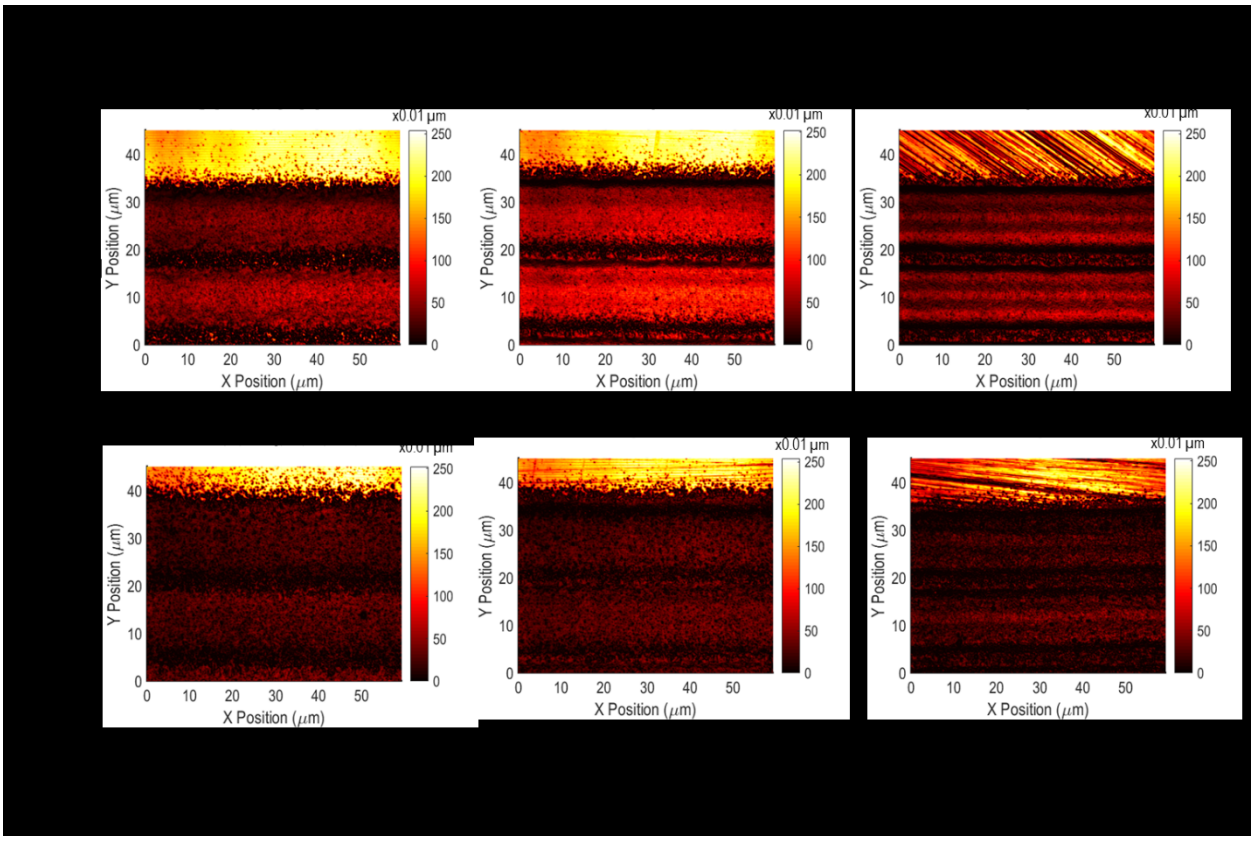
x0.01 µm
Y Position (µm)
X Position (µm)
0 10 20 30 40 50
0 10 20 30 40
250 200 150 100 50 0

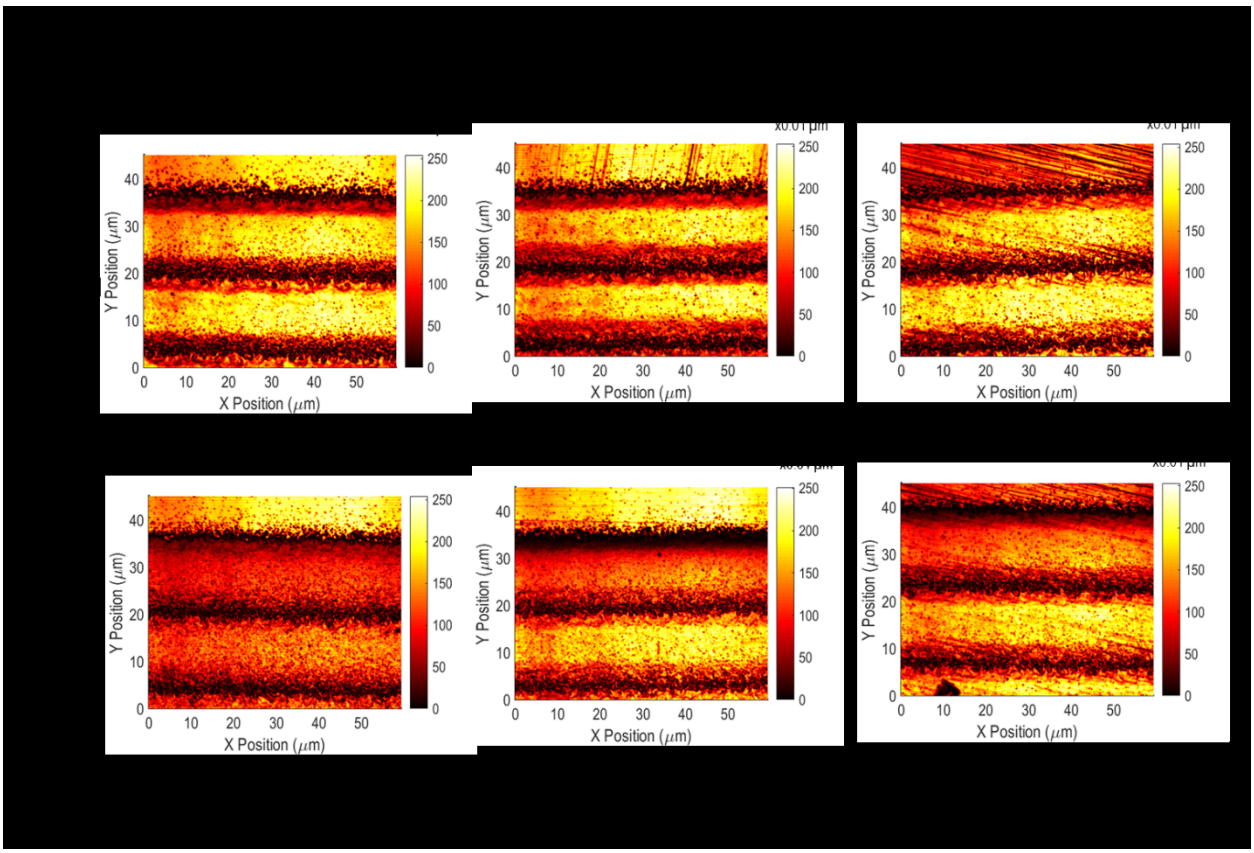
Y Position (µm)
X Position (µm)
0 10 20 30 40 50
0 10 20 30 40
250 200 150 100 50 0

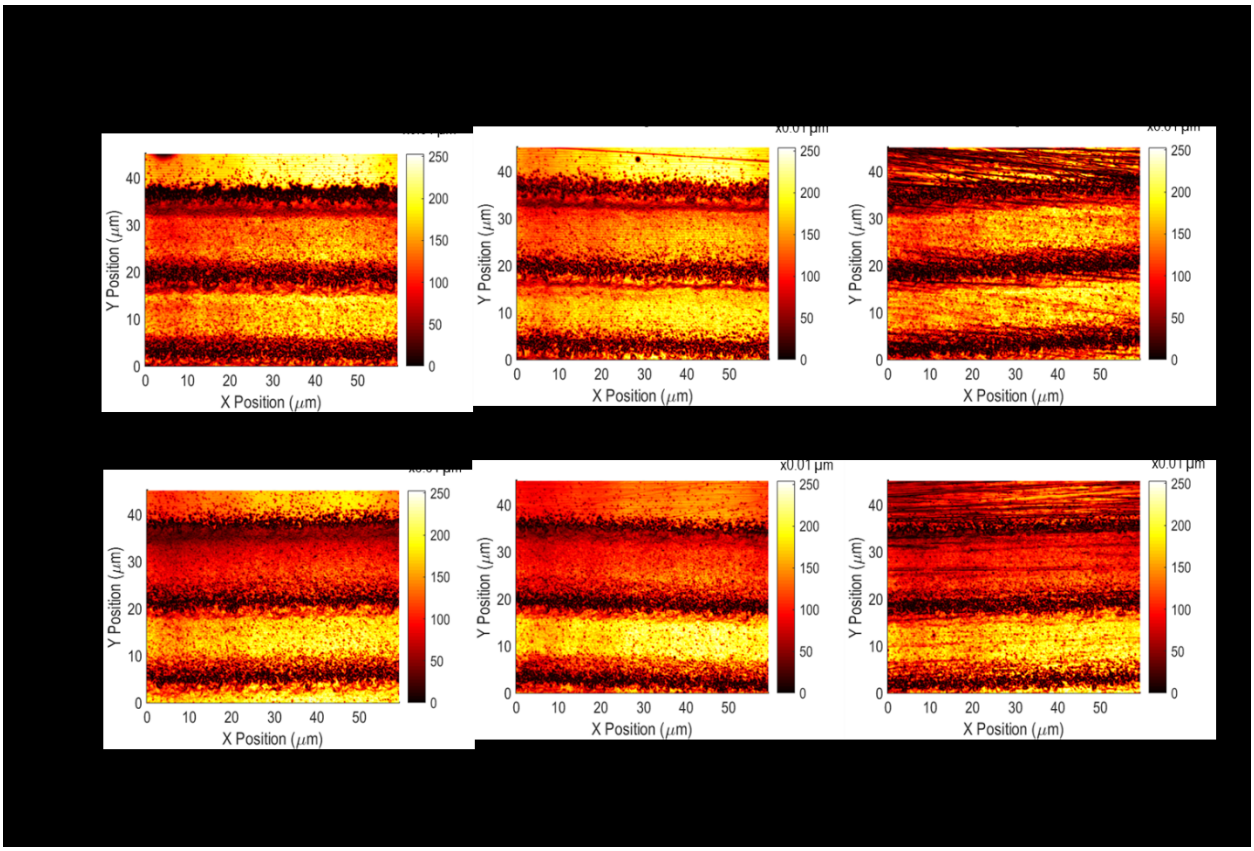
Y Position (μm)
X Position (μm)
x0.01 μm

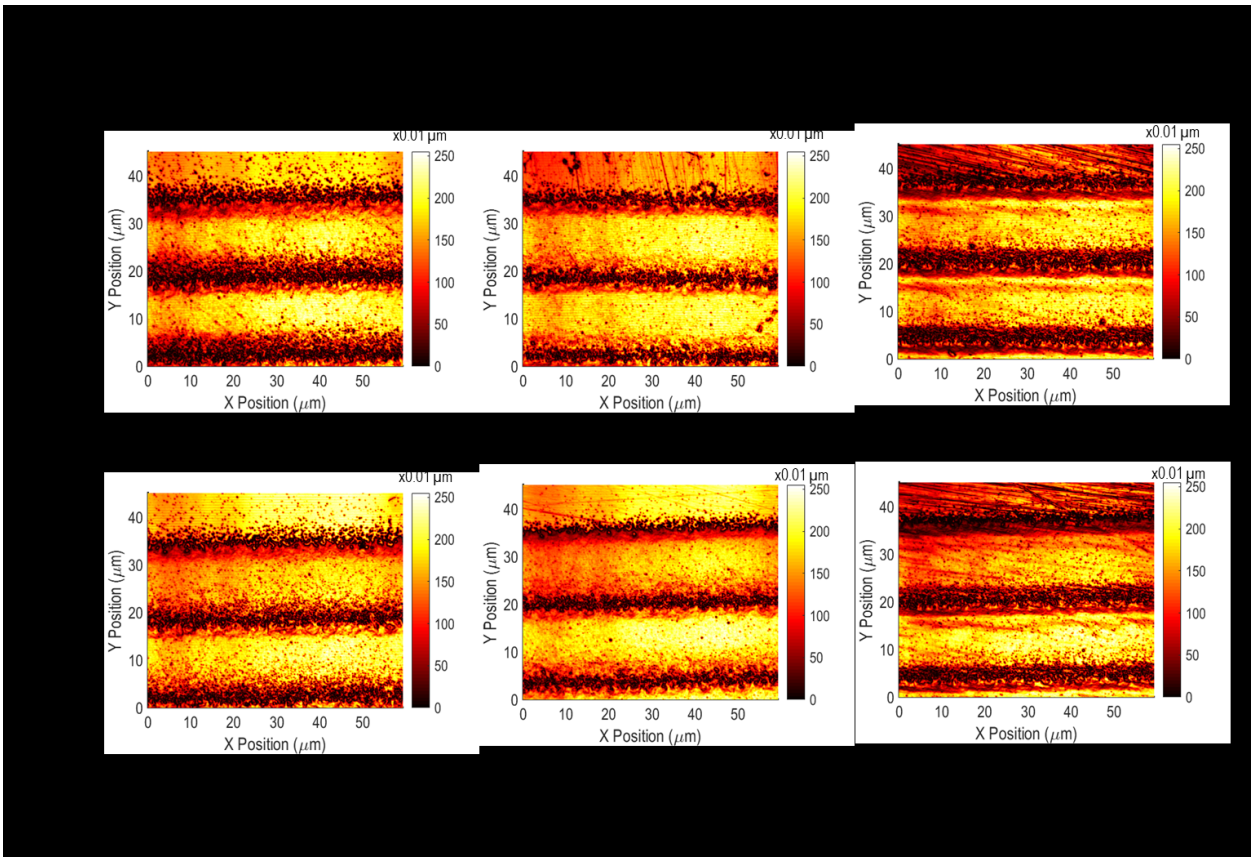
Y Position (μm)
X Position (μm)
x0.01 μm

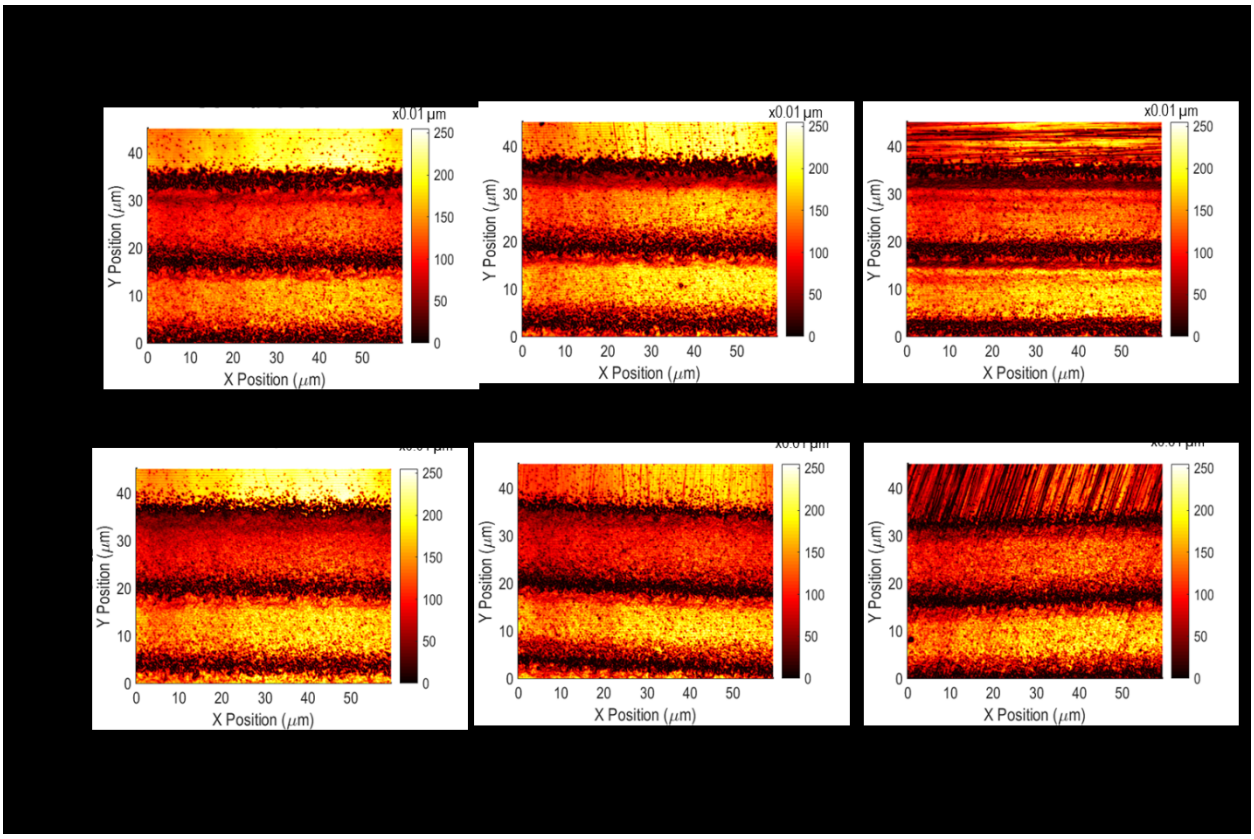
x0.01 μm
Y Position (μm)
X Position (μm)
0
10
20
30
40
50
250
200
150
100
50
0

Page intentionally left blank

Appendix B

Optical Micrographs of Laser-induced Ablation/Sensor Removal in All Samples in Test Matrix

Page intentionally left blank

Appendix B

Optical Micrographs of Laser-induced Ablation/Sensor Removal in All Samples in Test Matrix

Sample 001 – Damage at 4 µJ

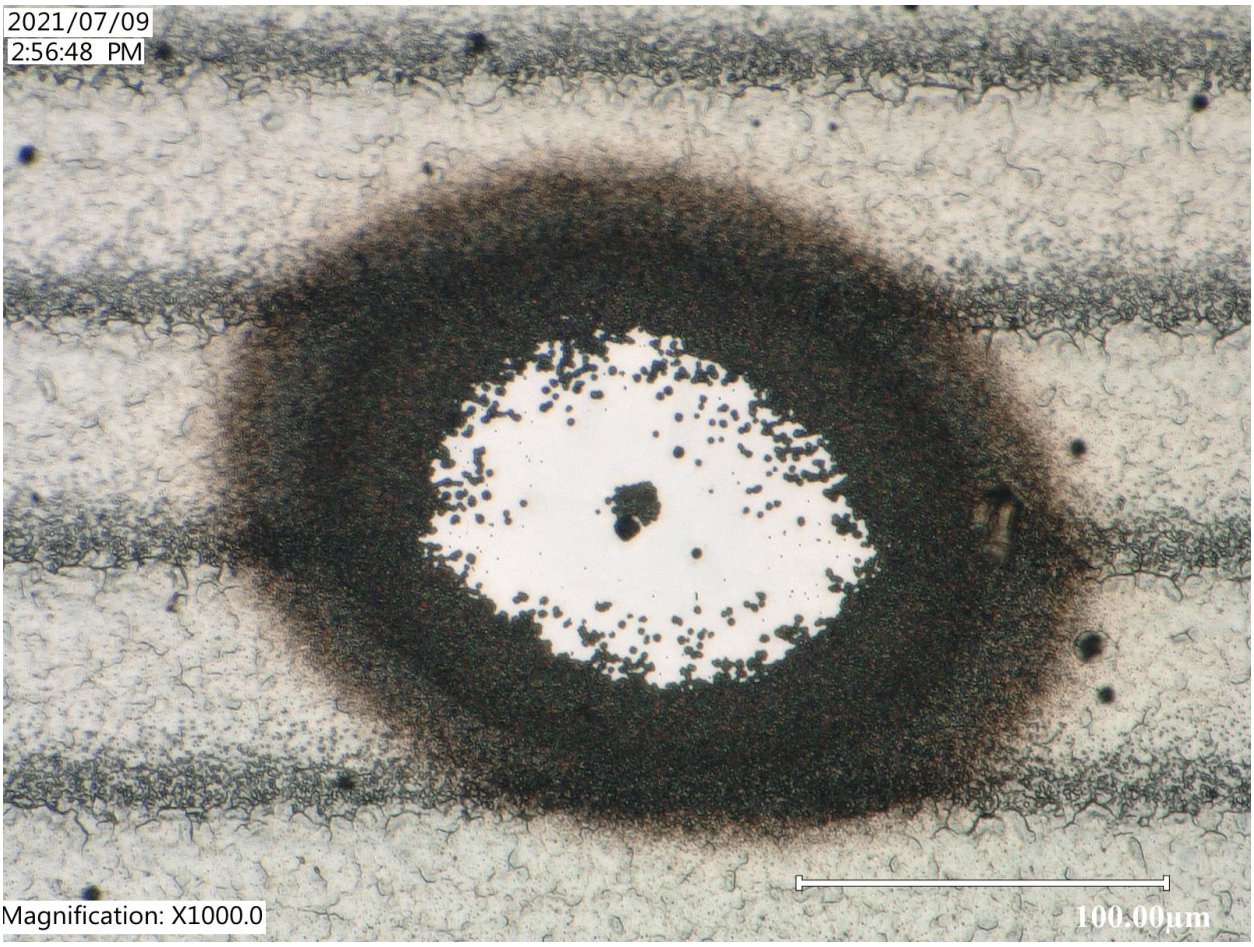

Sample 002 – Damage at 4 µJ

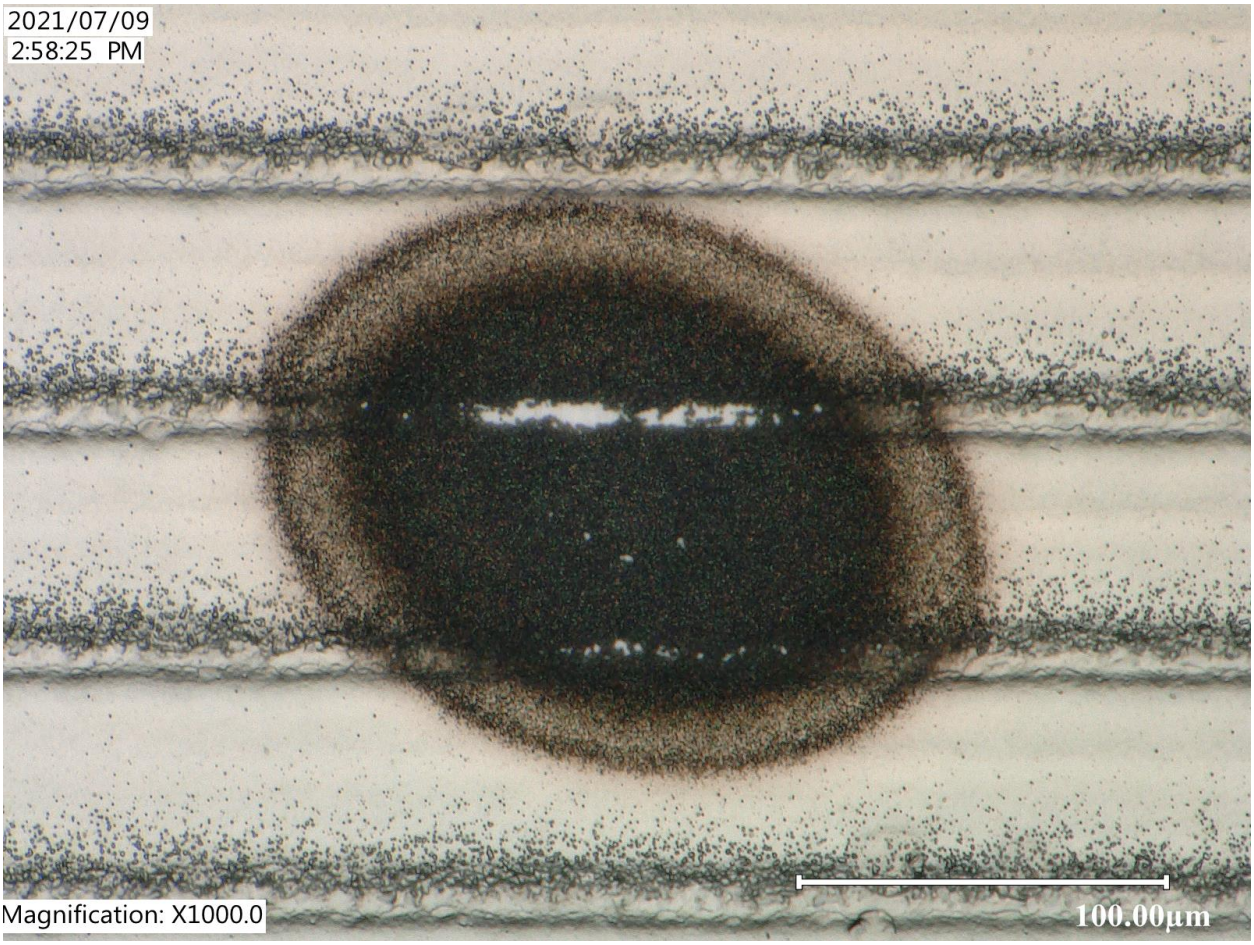

Sample 003 – Damage at 4 µJ

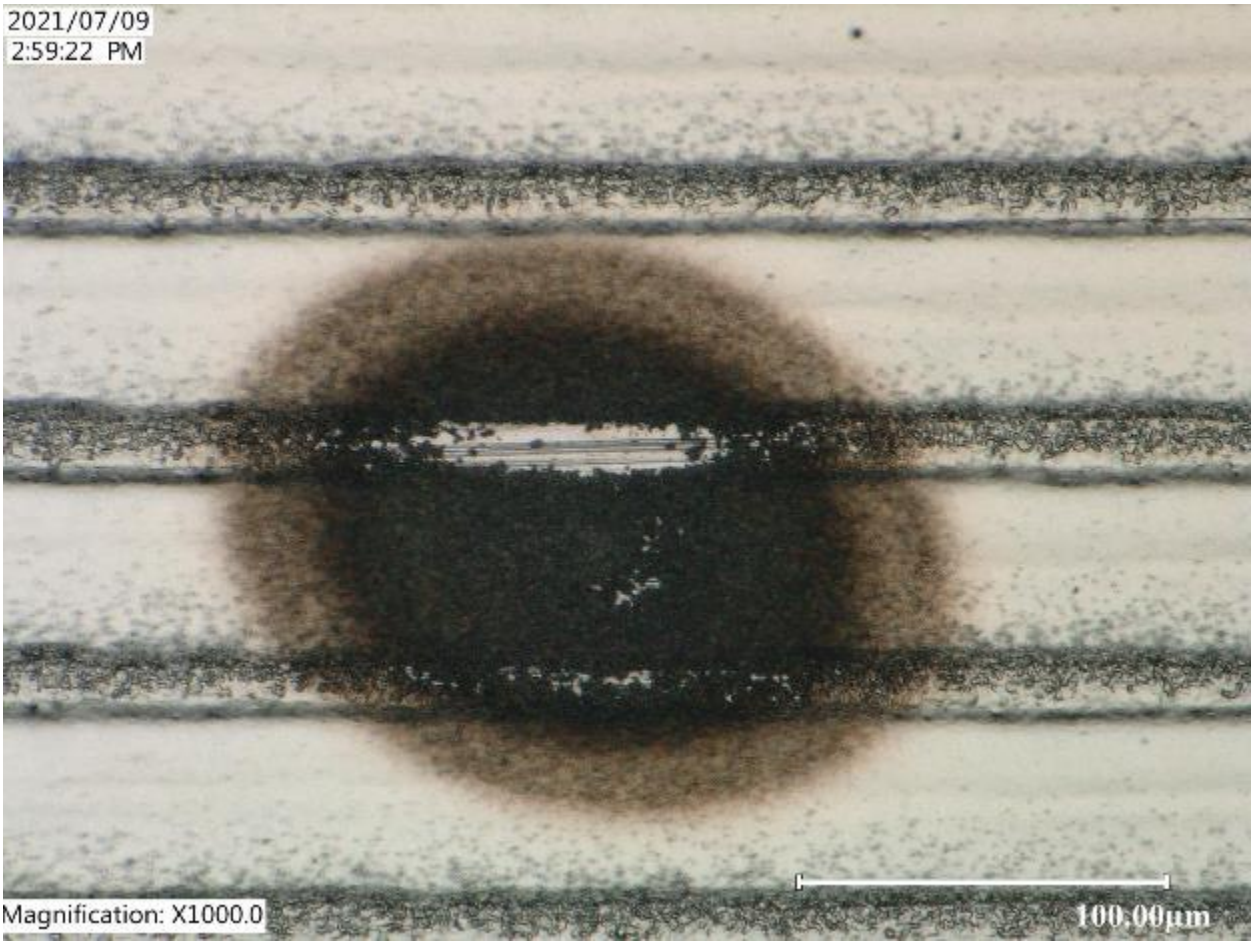

Sample 004 – Damage at 4 µJ

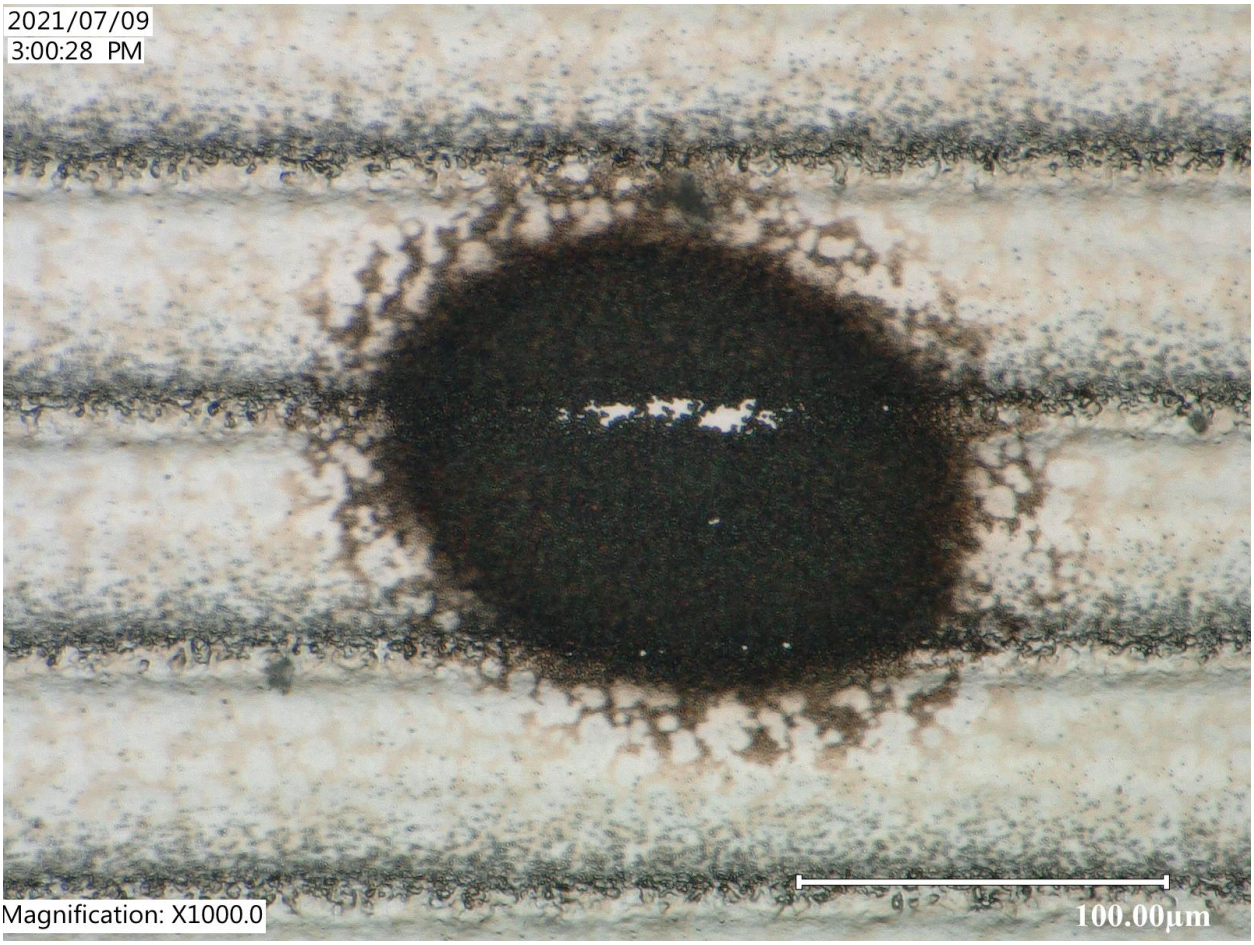

Sample 005 – Damage at 4 µJ

Sample 006 – Damage at 4 µJ

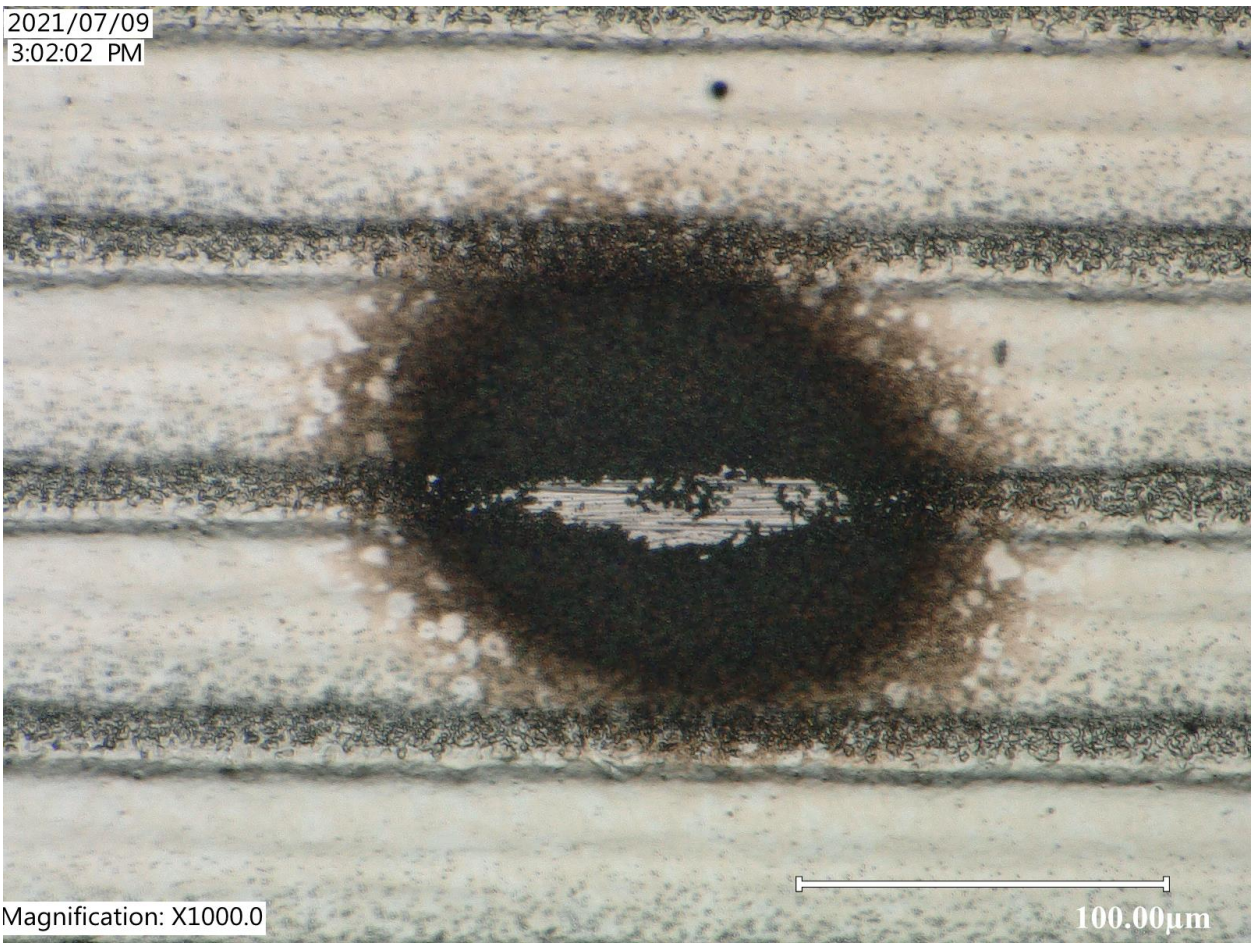

Sample 007 – Damage at 6 µJ

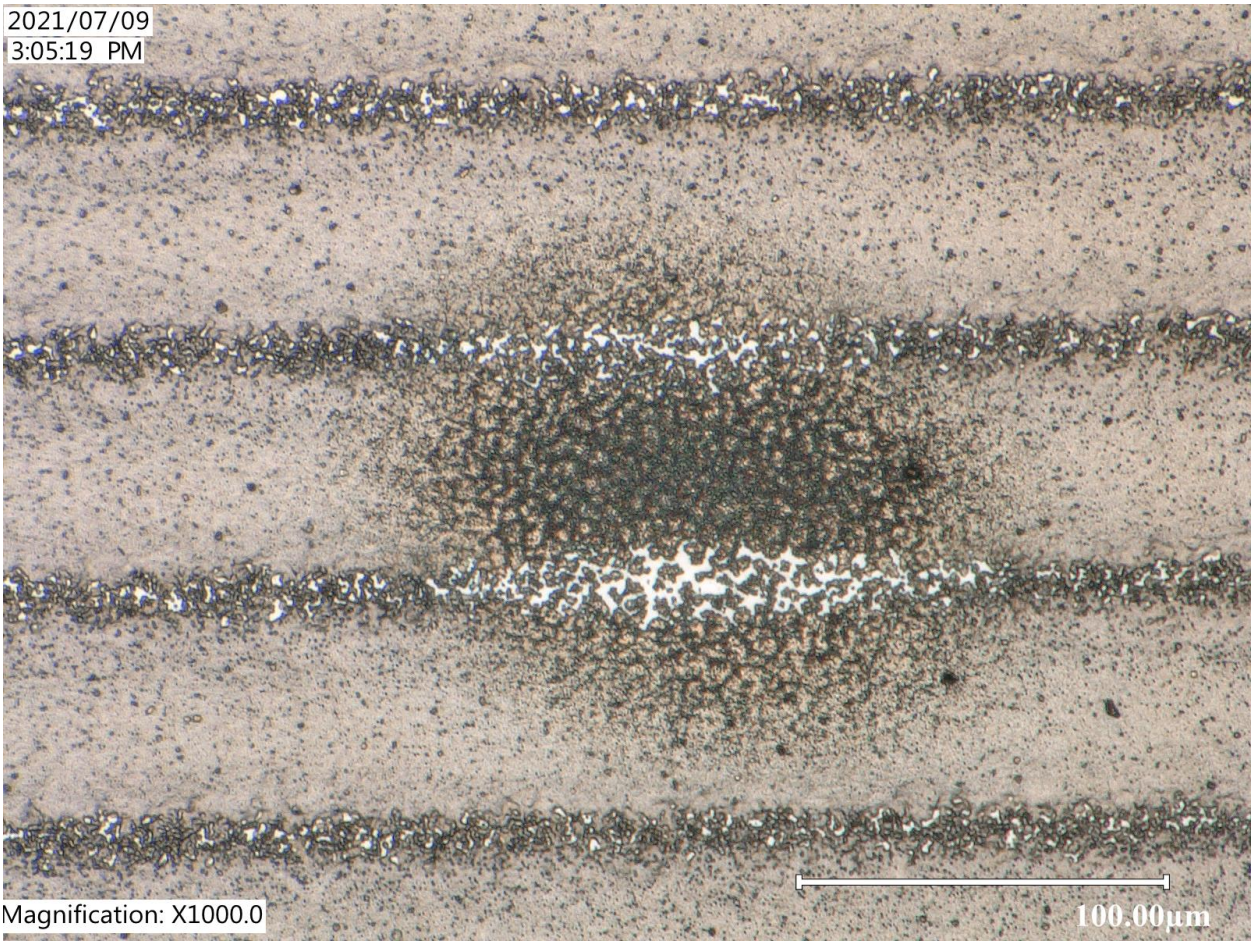

Sample 008 – Damage at 6 µJ

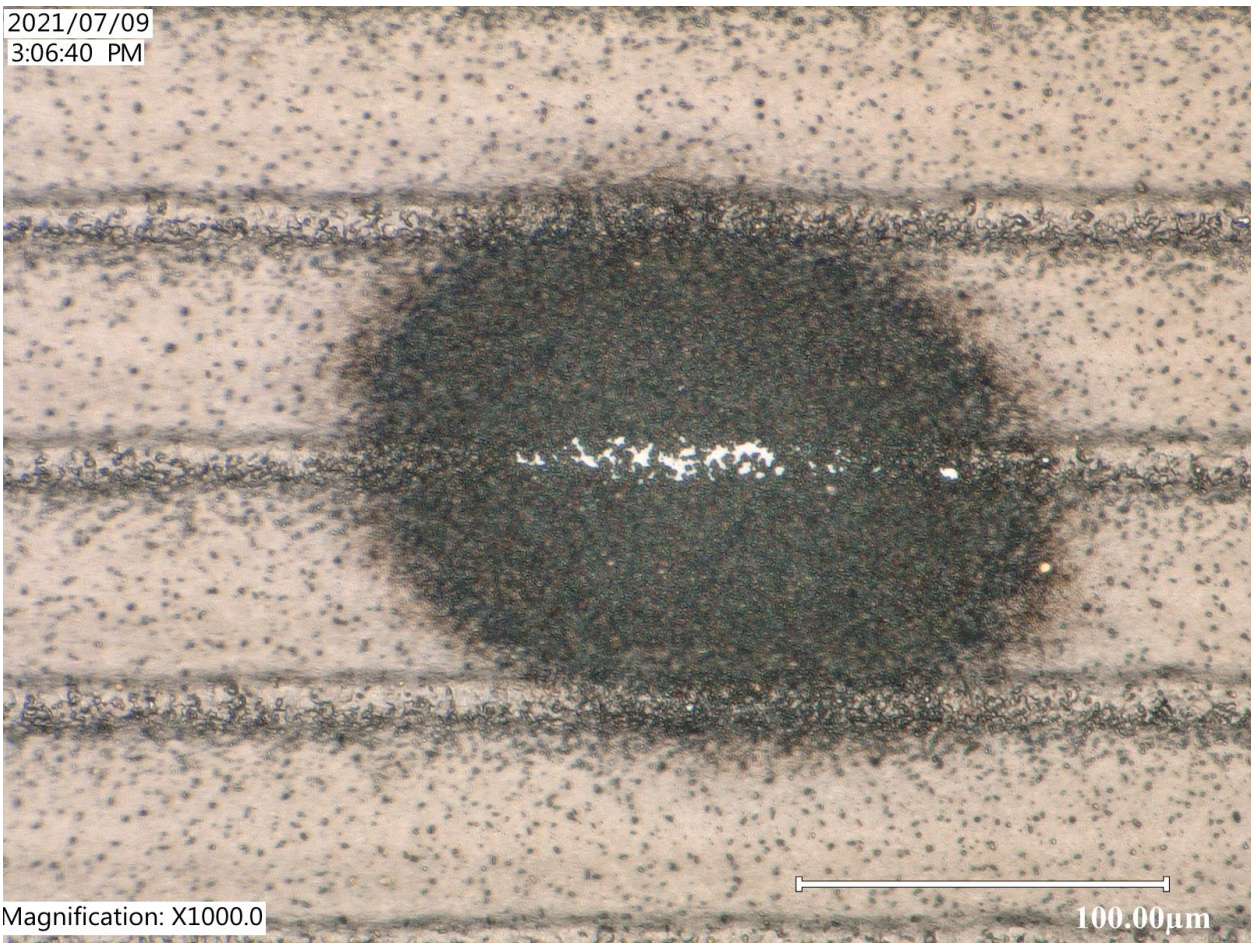

Sample 009 – Damage at 8 µJ

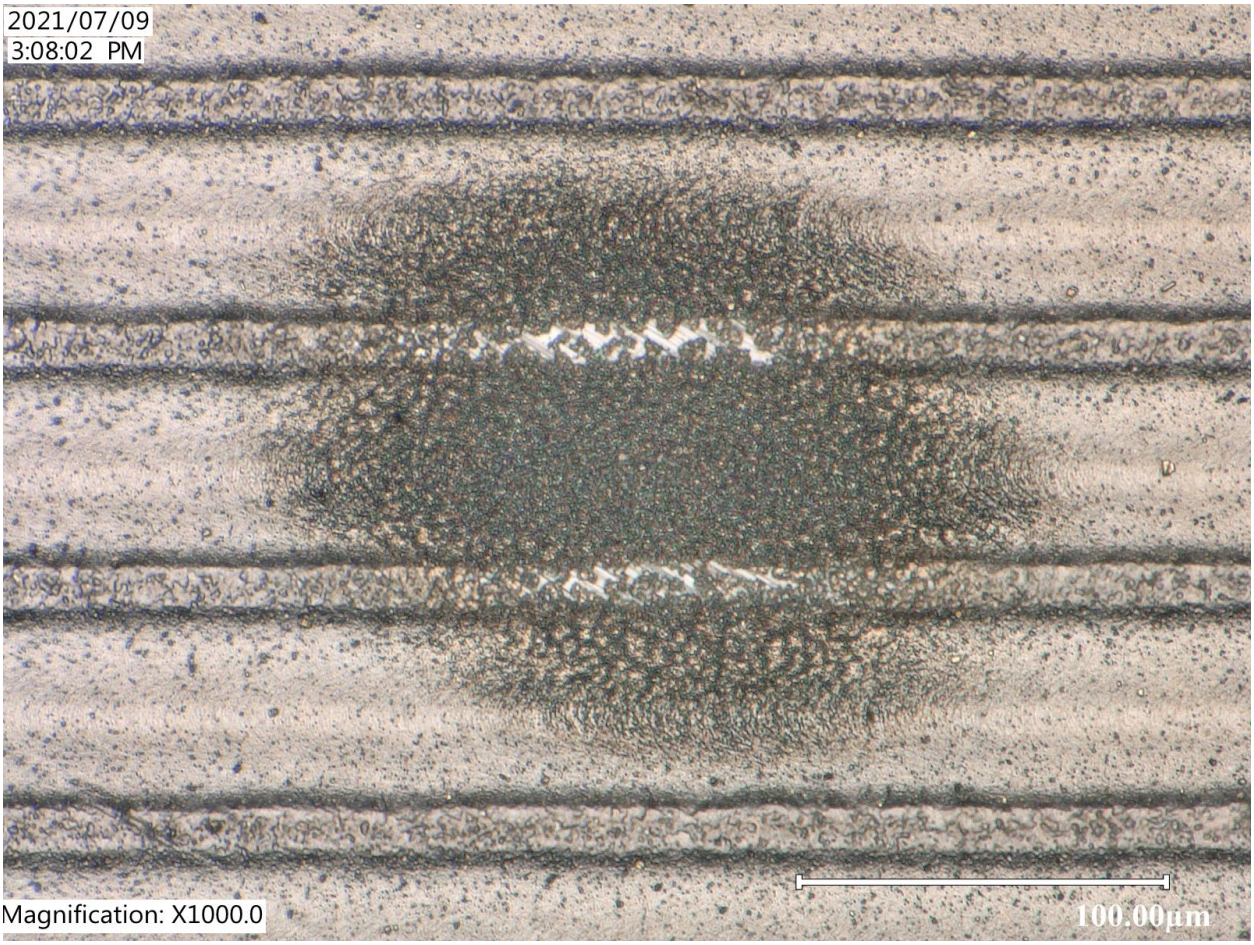

Sample 010 – Damage at 8 µJ

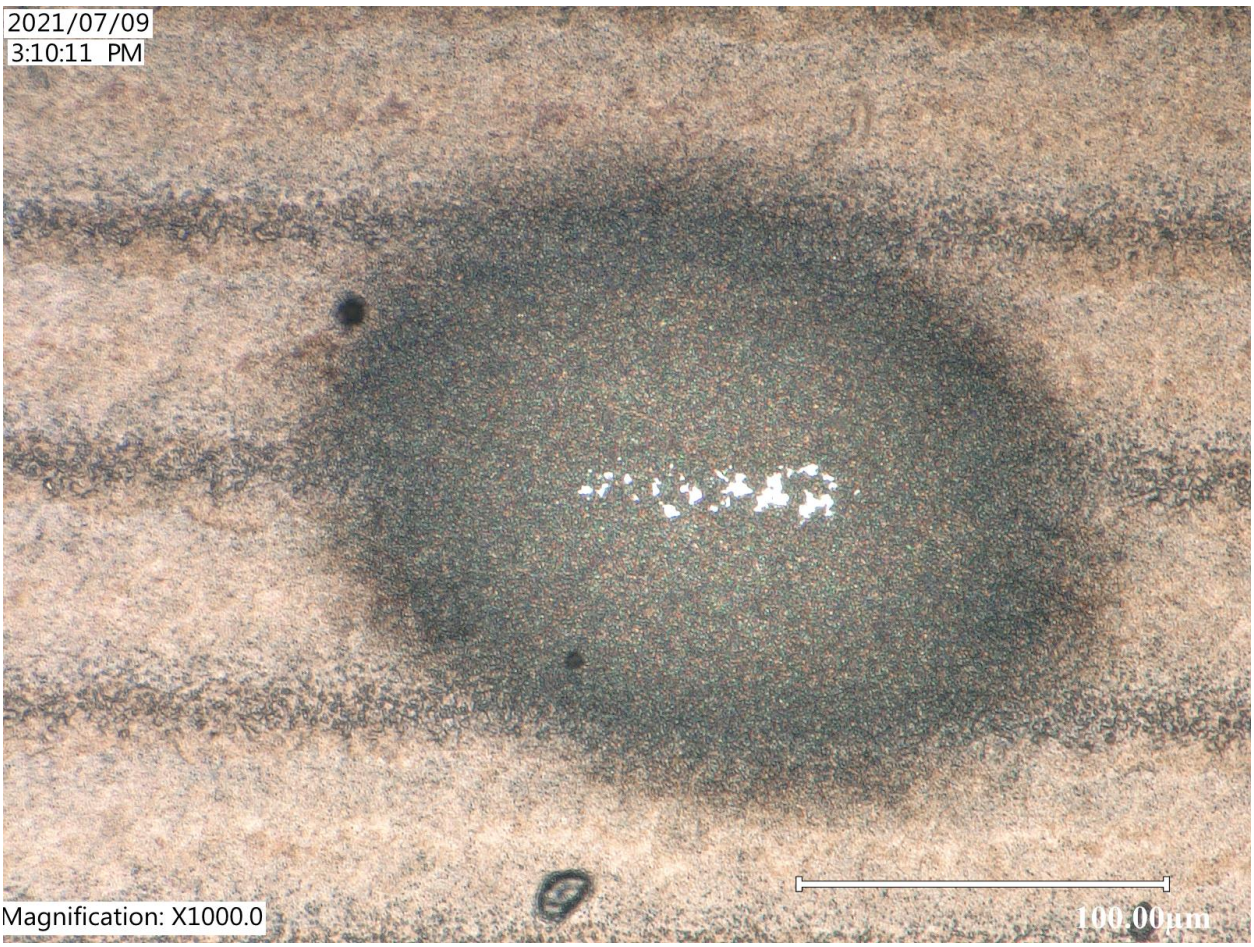

Sample 011 – Damage at 8 µJ

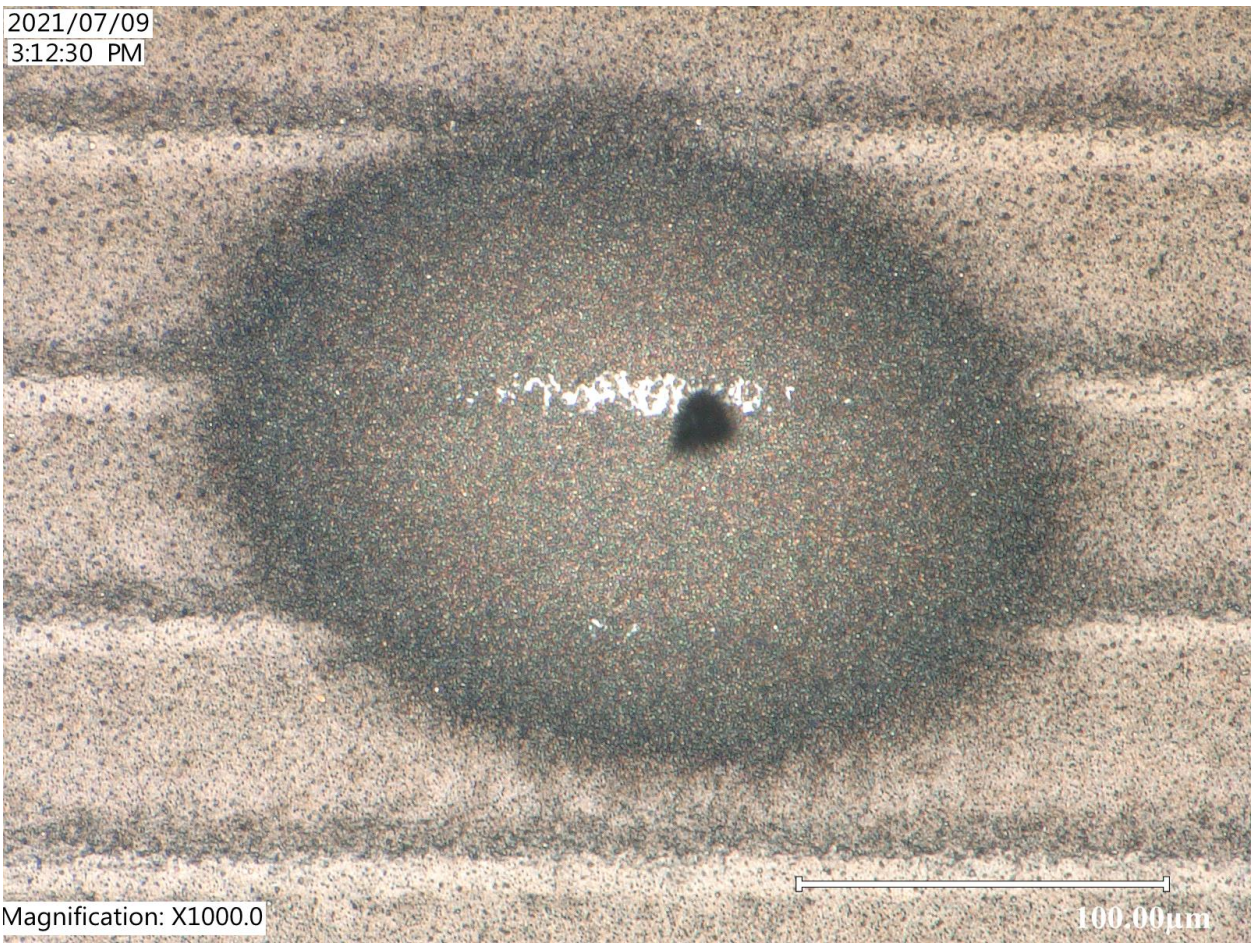

Sample 012 – Damage at 8 µJ

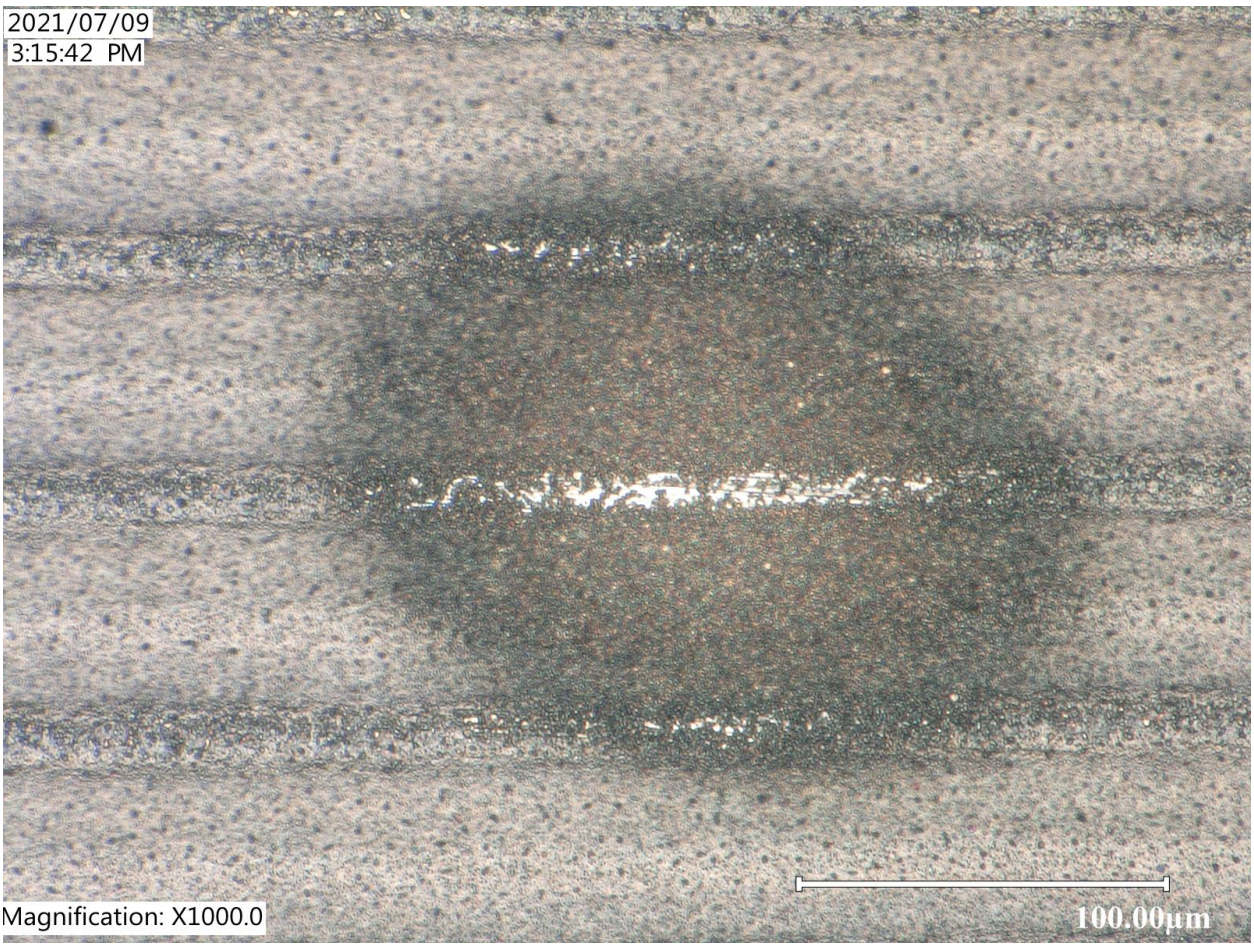

Sample 013 – Damage at 4 µJ

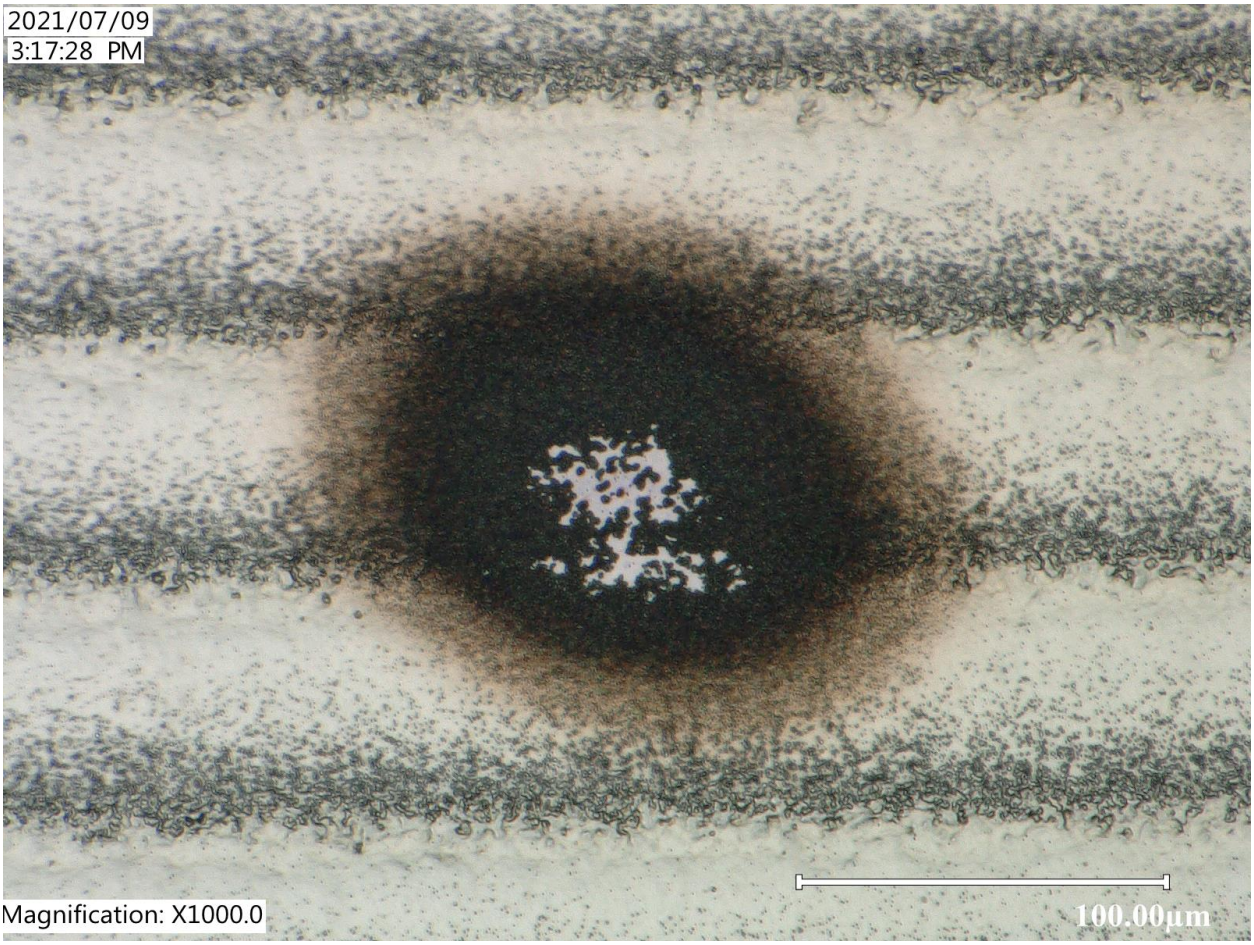

Sample 014 – Damage at 4 µJ

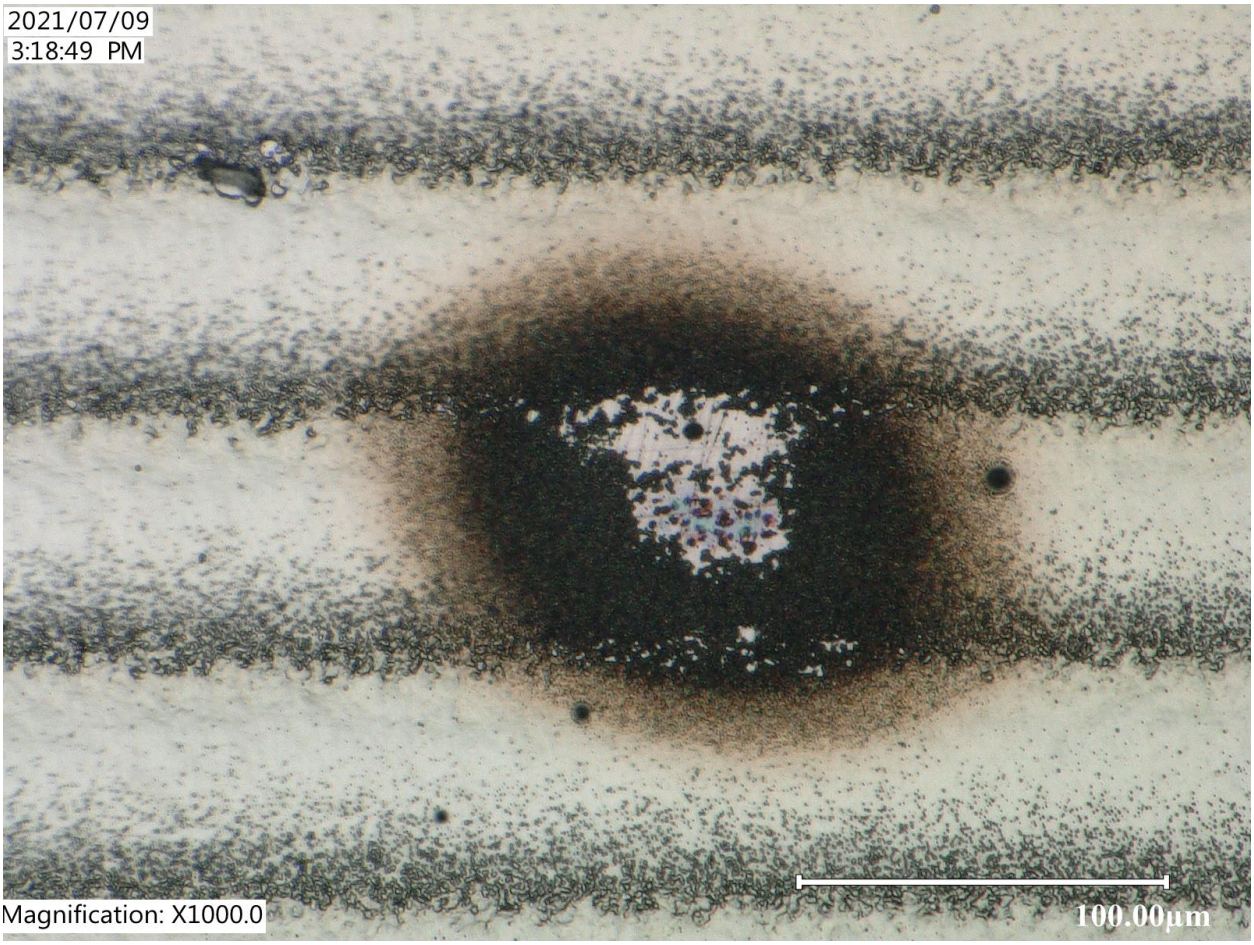

Sample 015 – Damage at 4 µJ

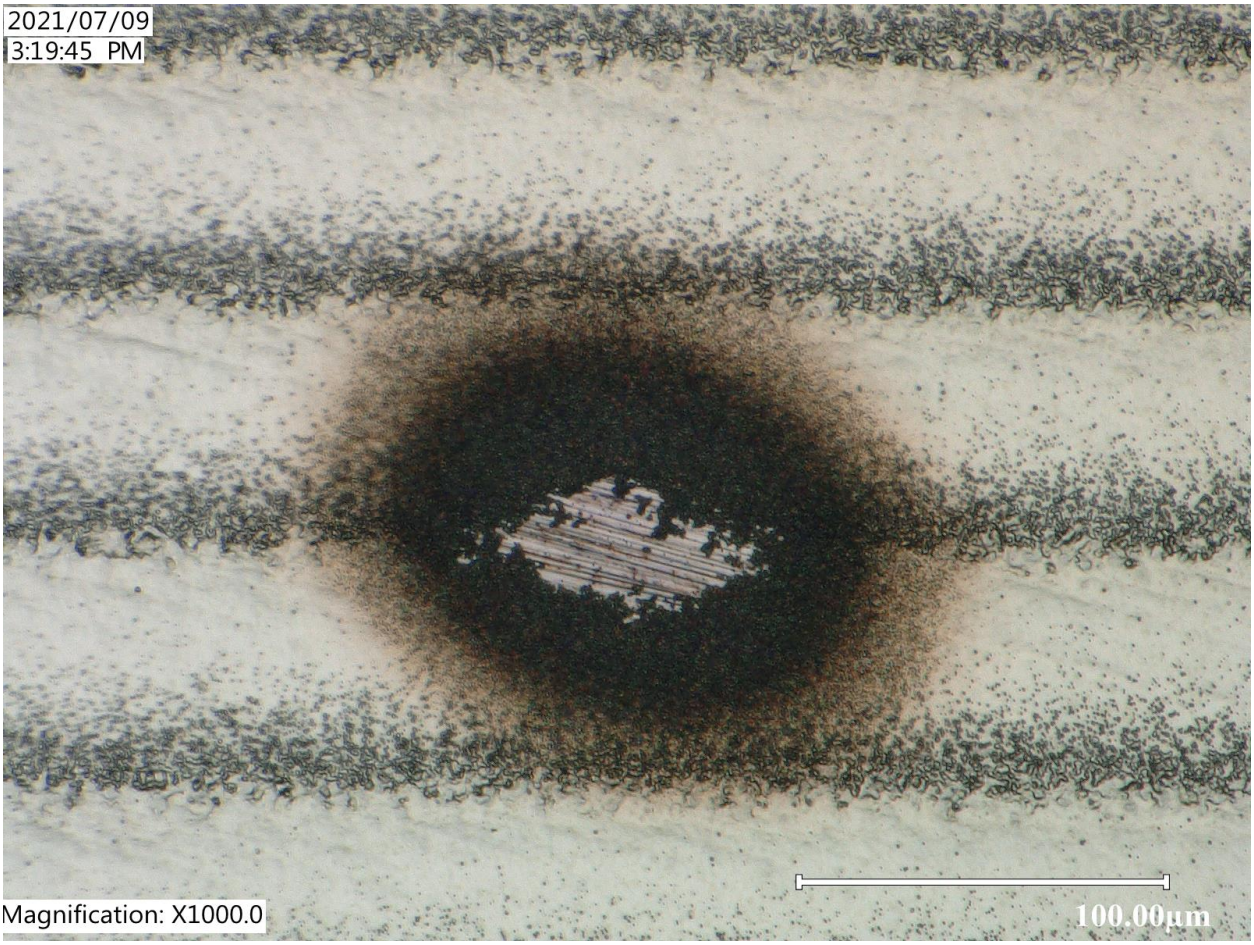

Sample 016 – Damage at 14 µJ

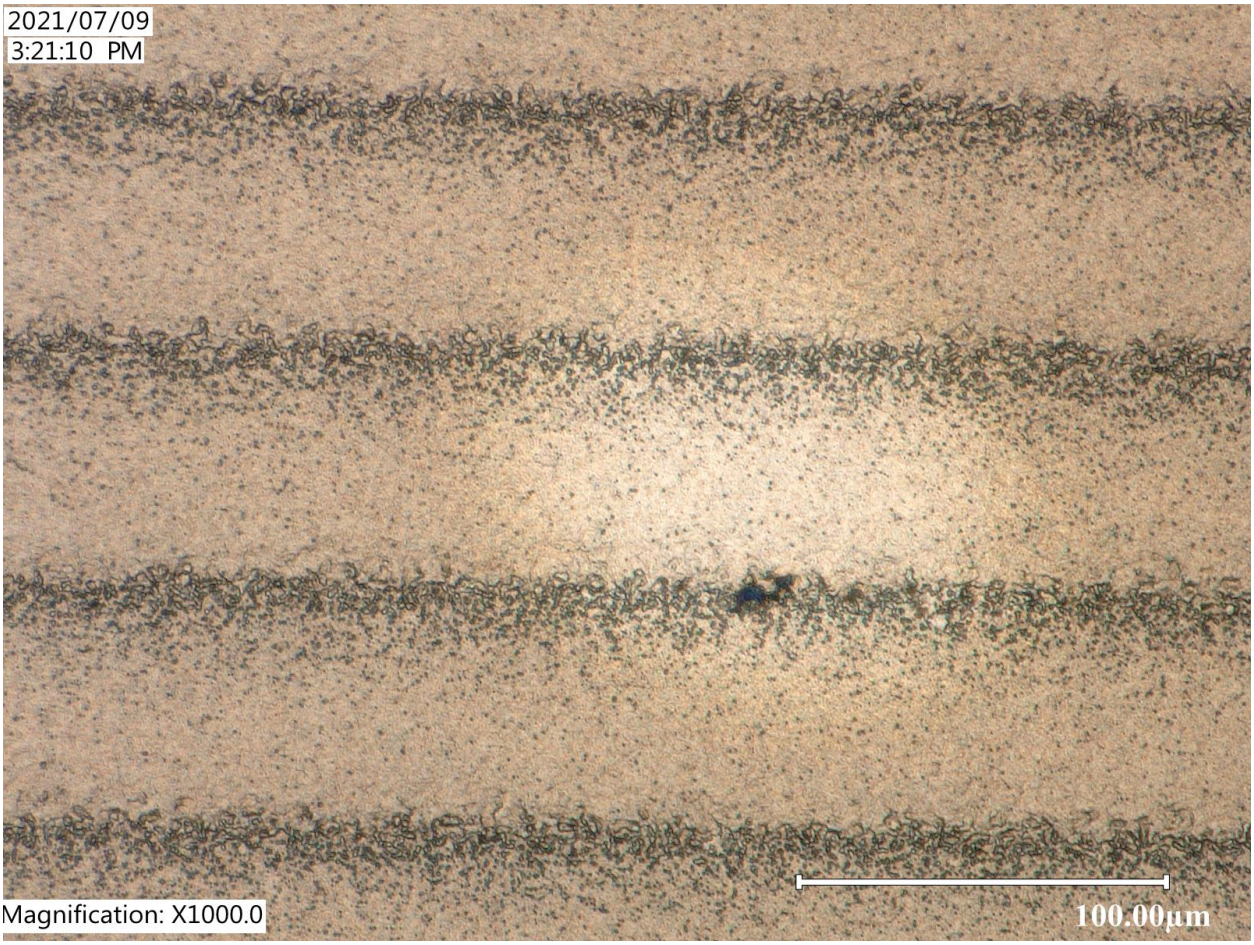

Sample 017 – Damage at 14 µJ

Sample 018 – Damage at 14 µJ

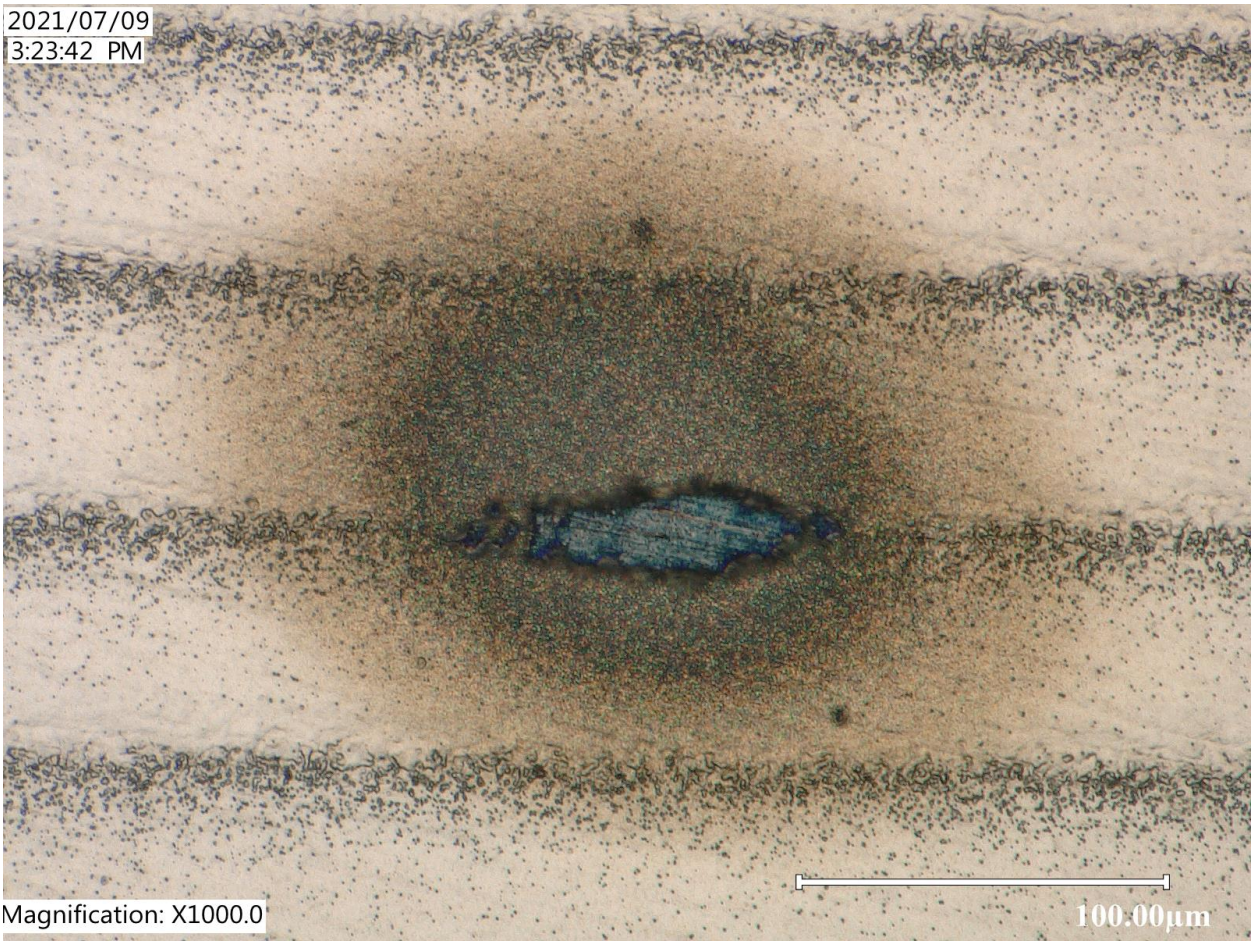

Sample 019 – Damage at 6 µJ

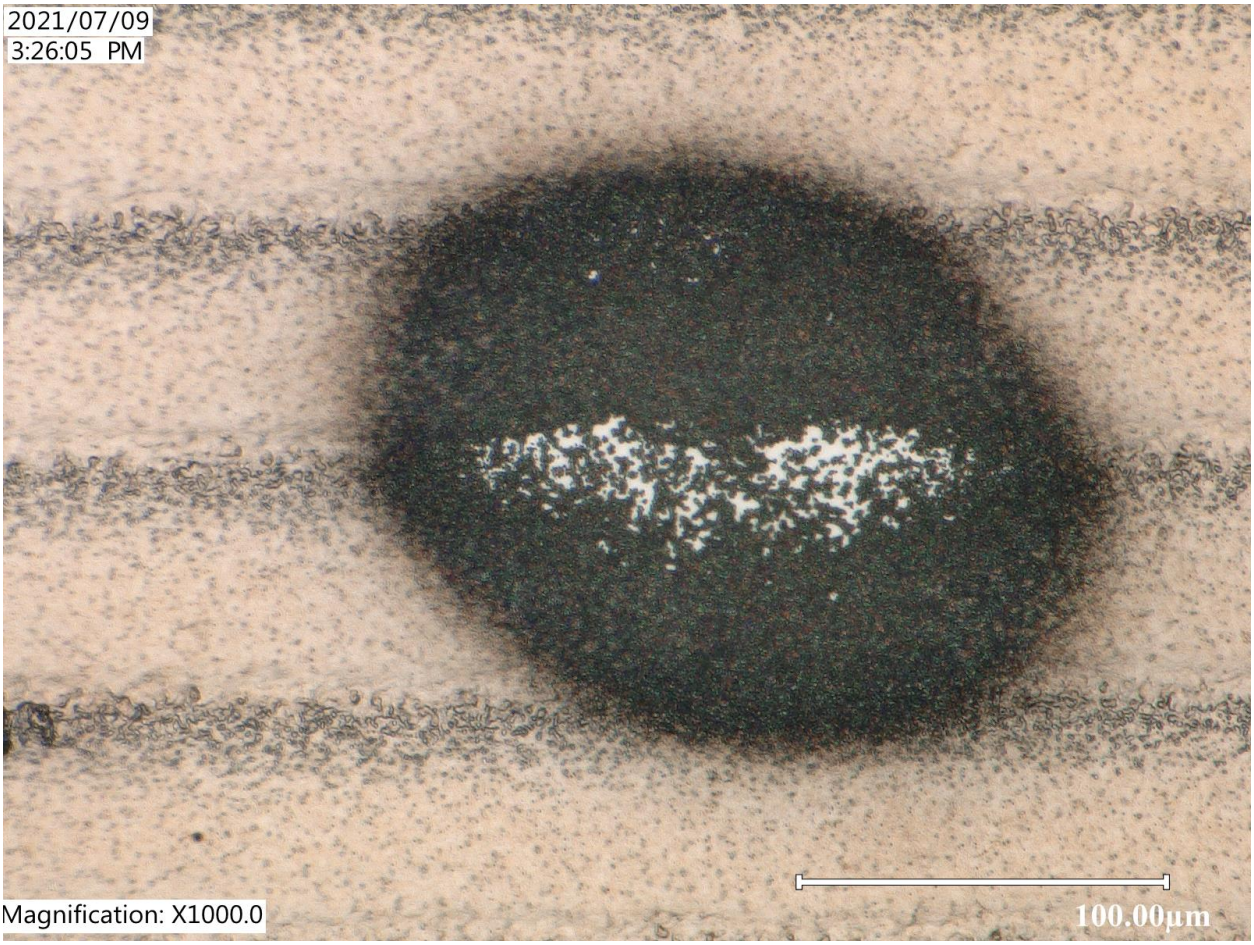

Sample 020 – Damage at 10 µJ

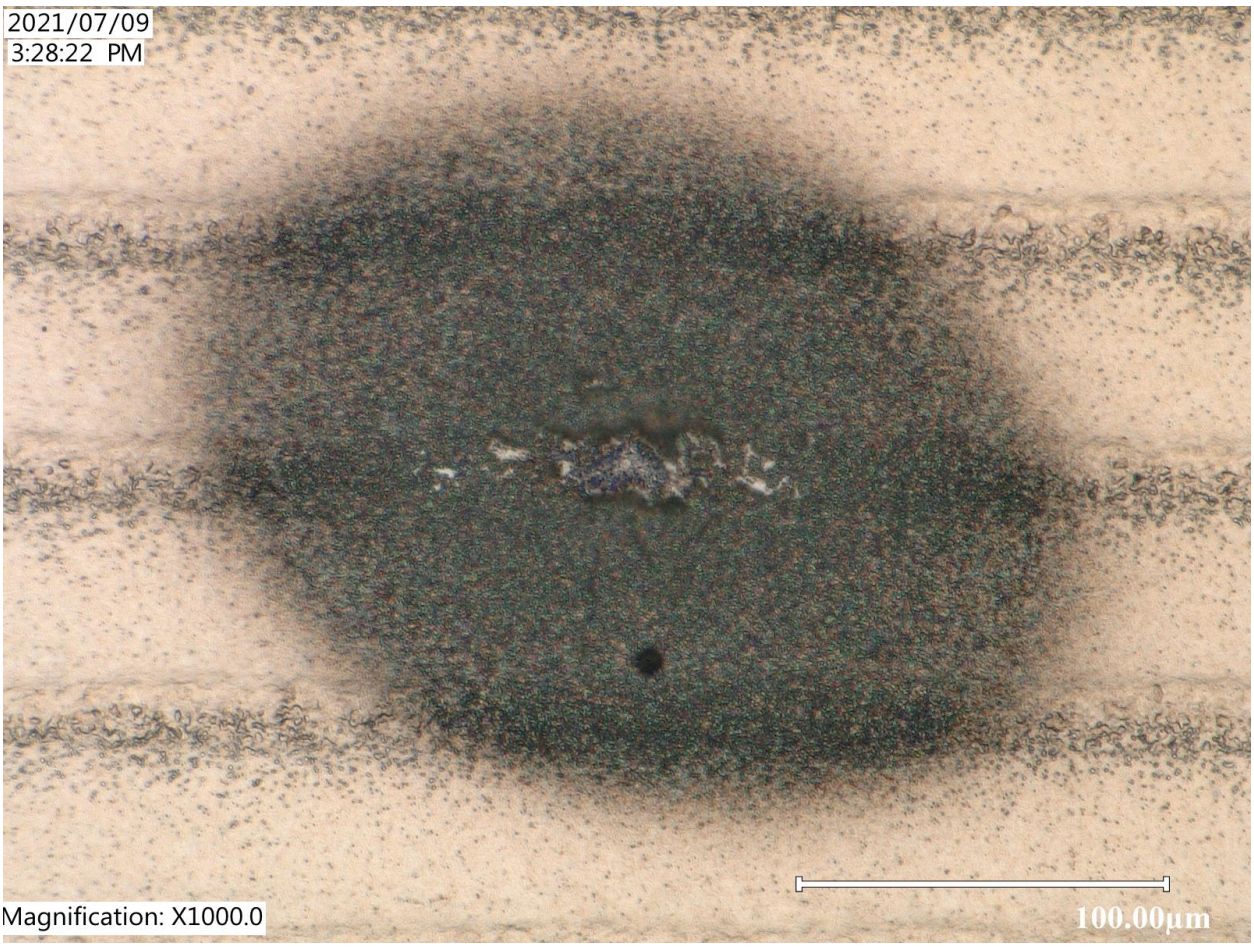

Sample 021 – Damage at 10 µJ

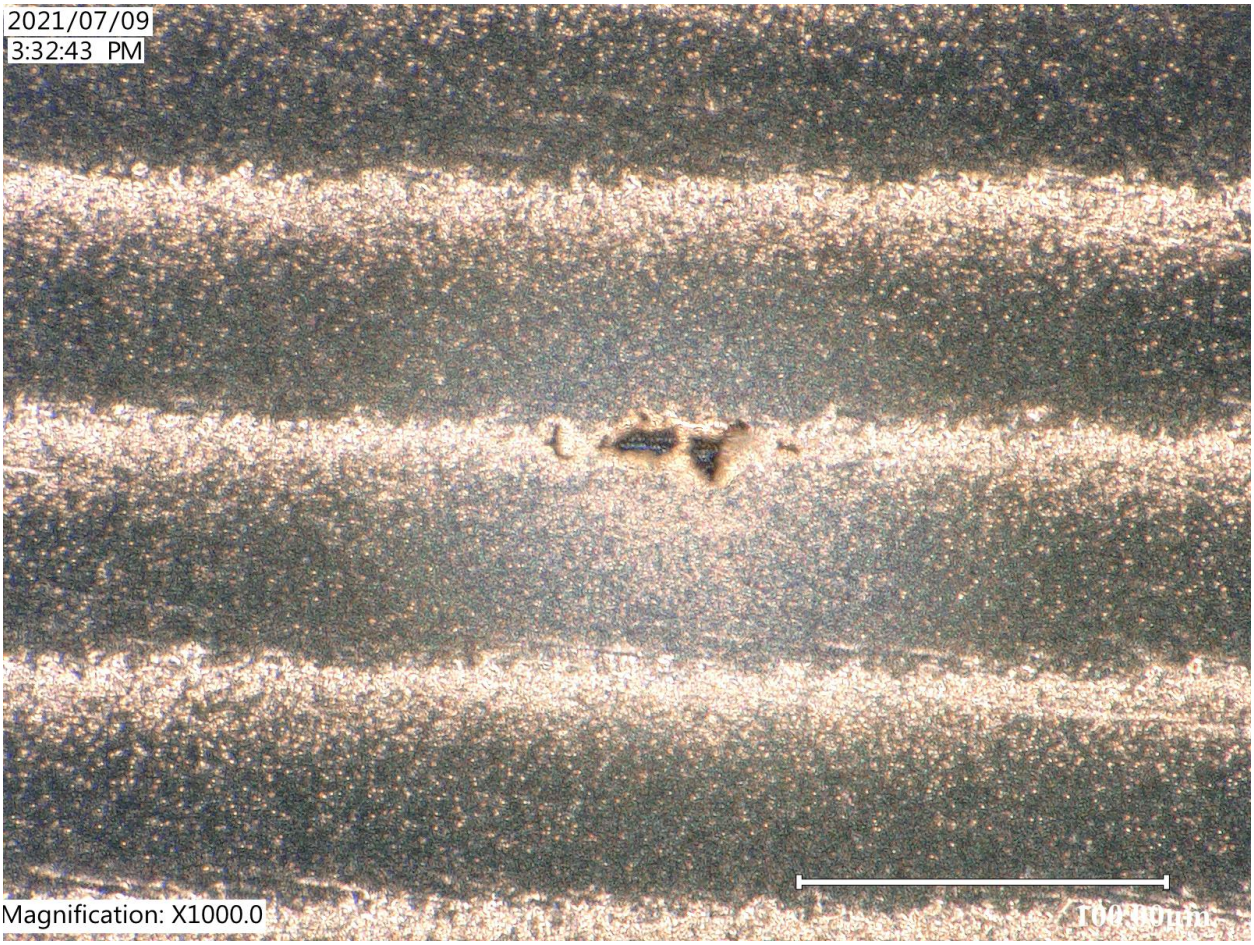

Sample 022 – No damage at 14 µJ

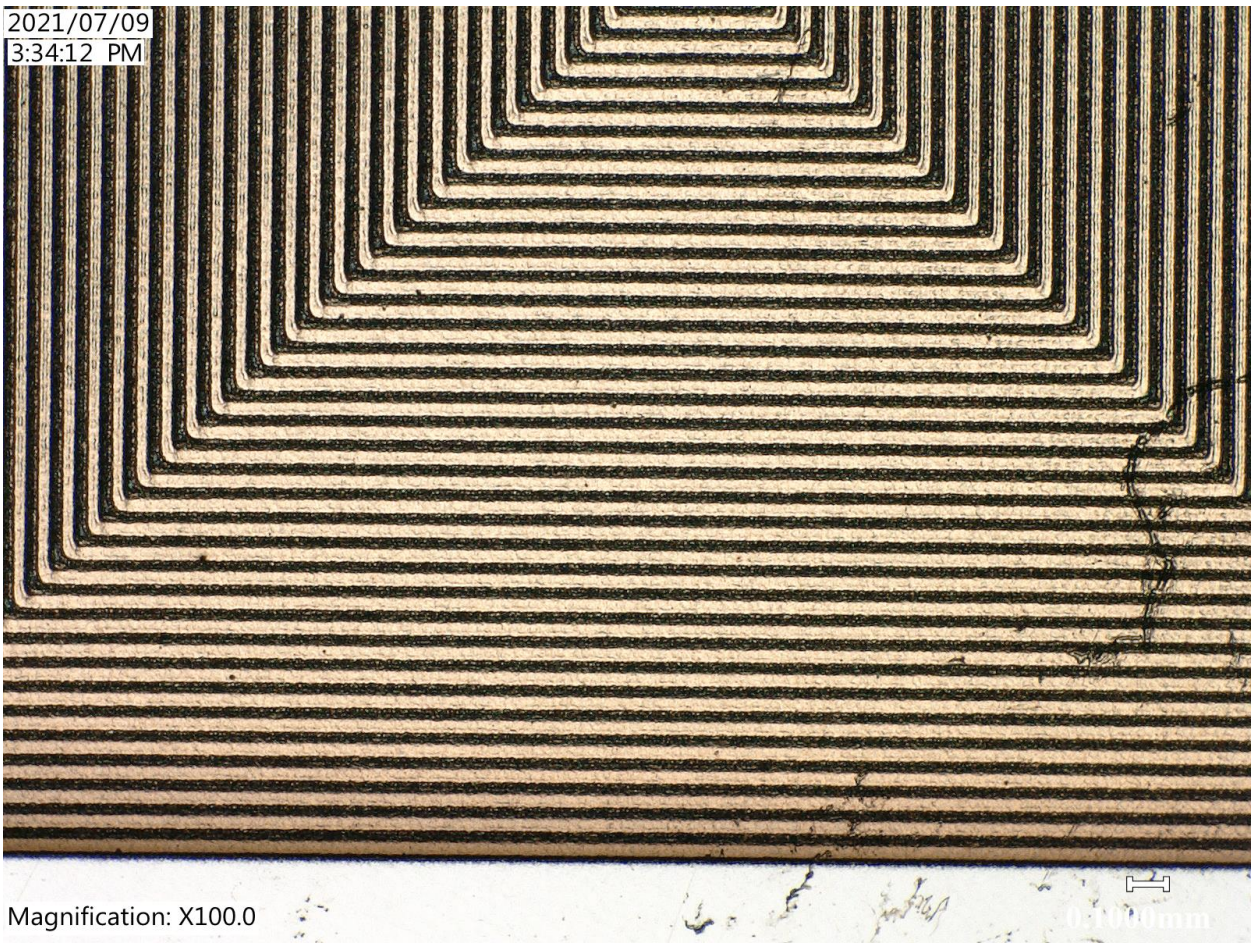

Sample 023 – No damage at 14 µJ

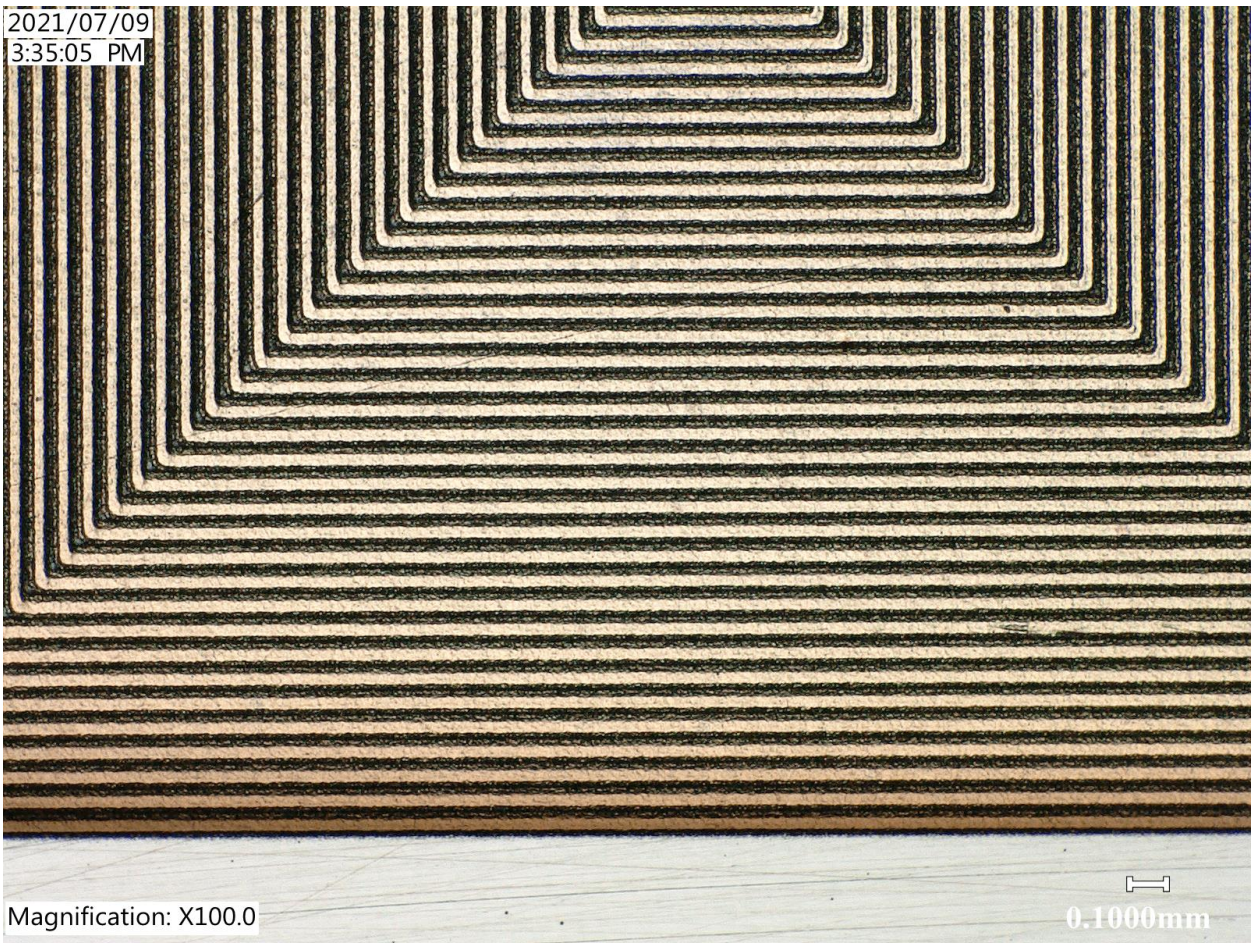

Sample 024 – No damage at 14 µJ

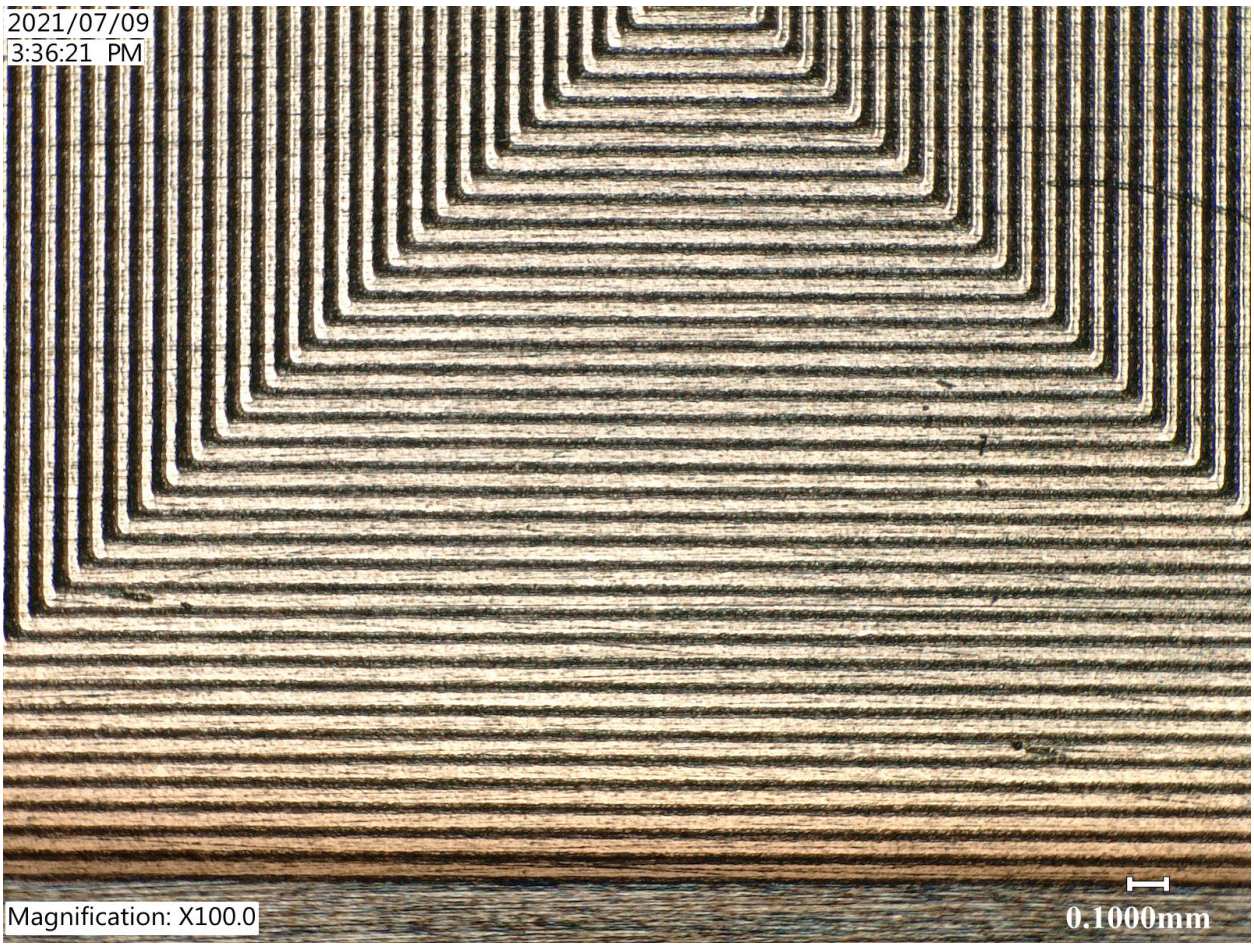

Sample 025 – Damage at 4 µJ

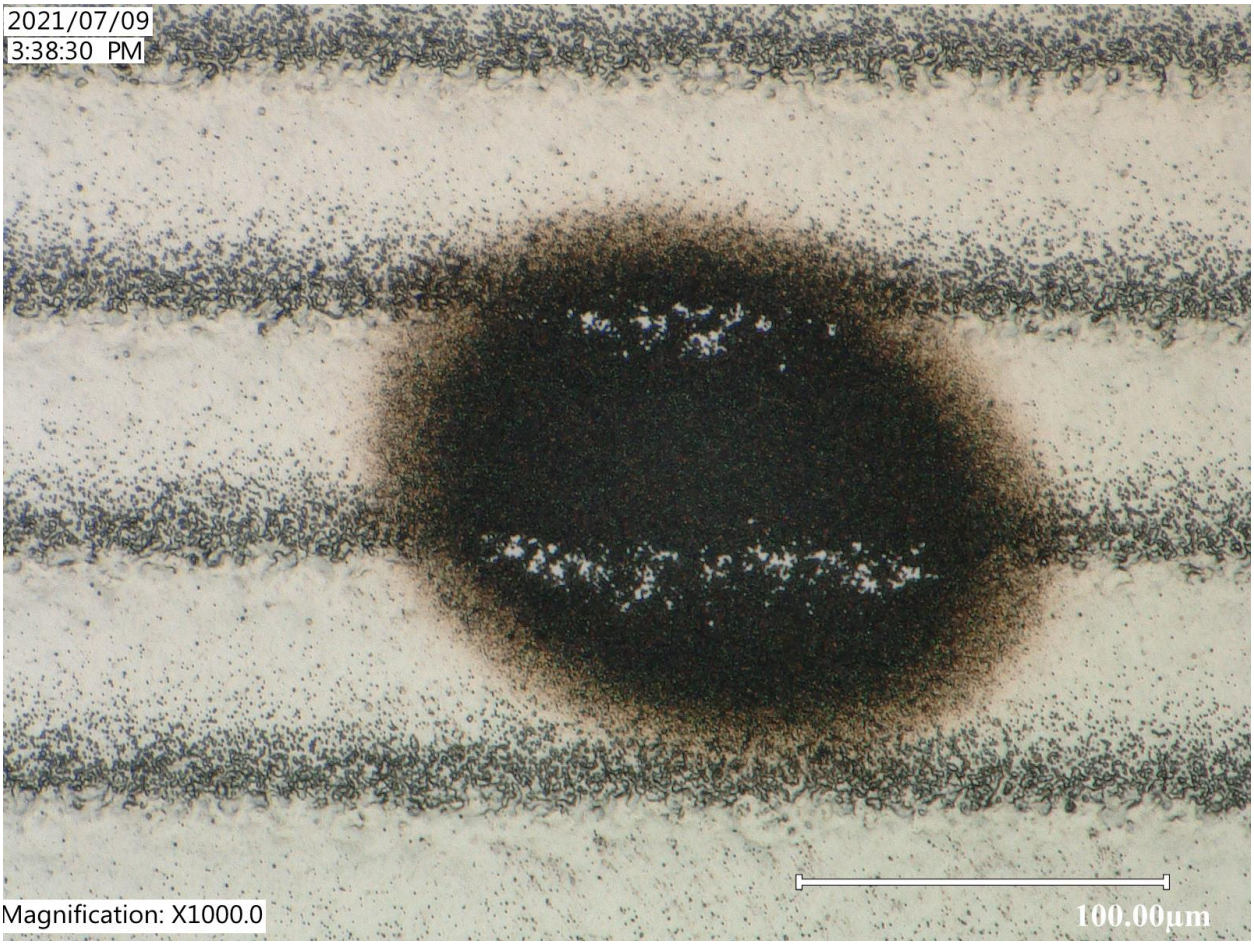

Sample 026 – Damage at 4 µJ

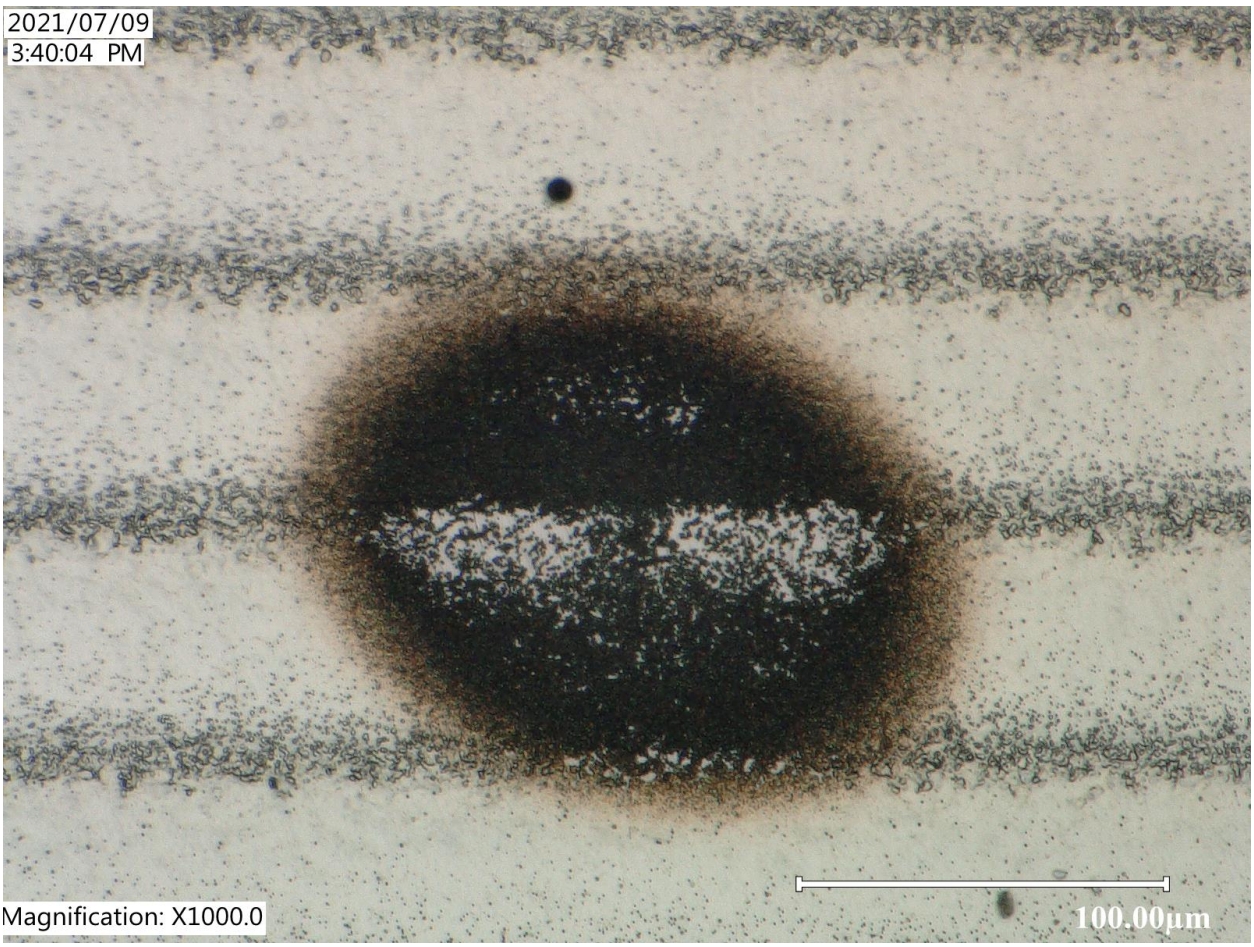

Sample 027 – Damage at 4 µJ

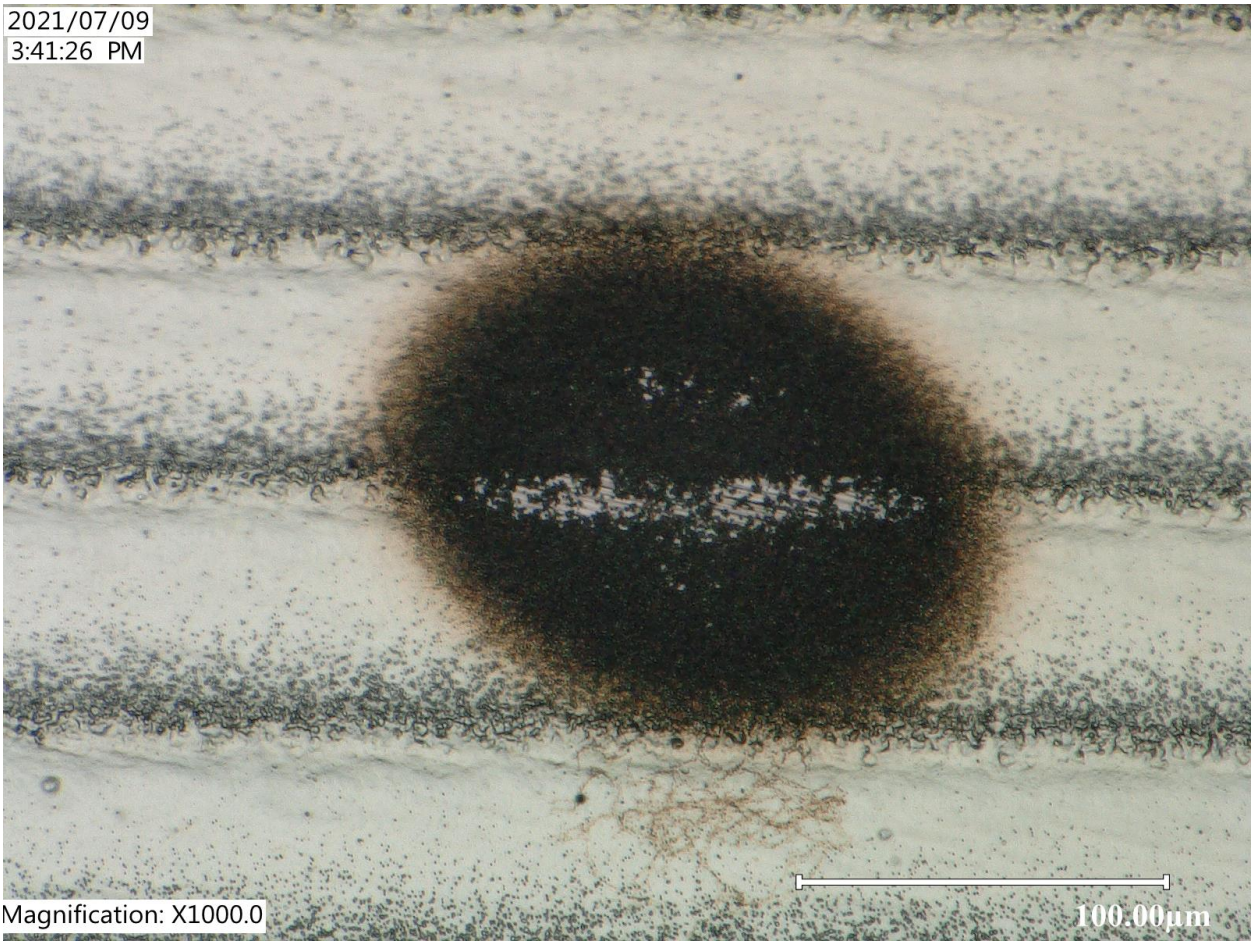

Sample 028 – Damage at 14 µJ

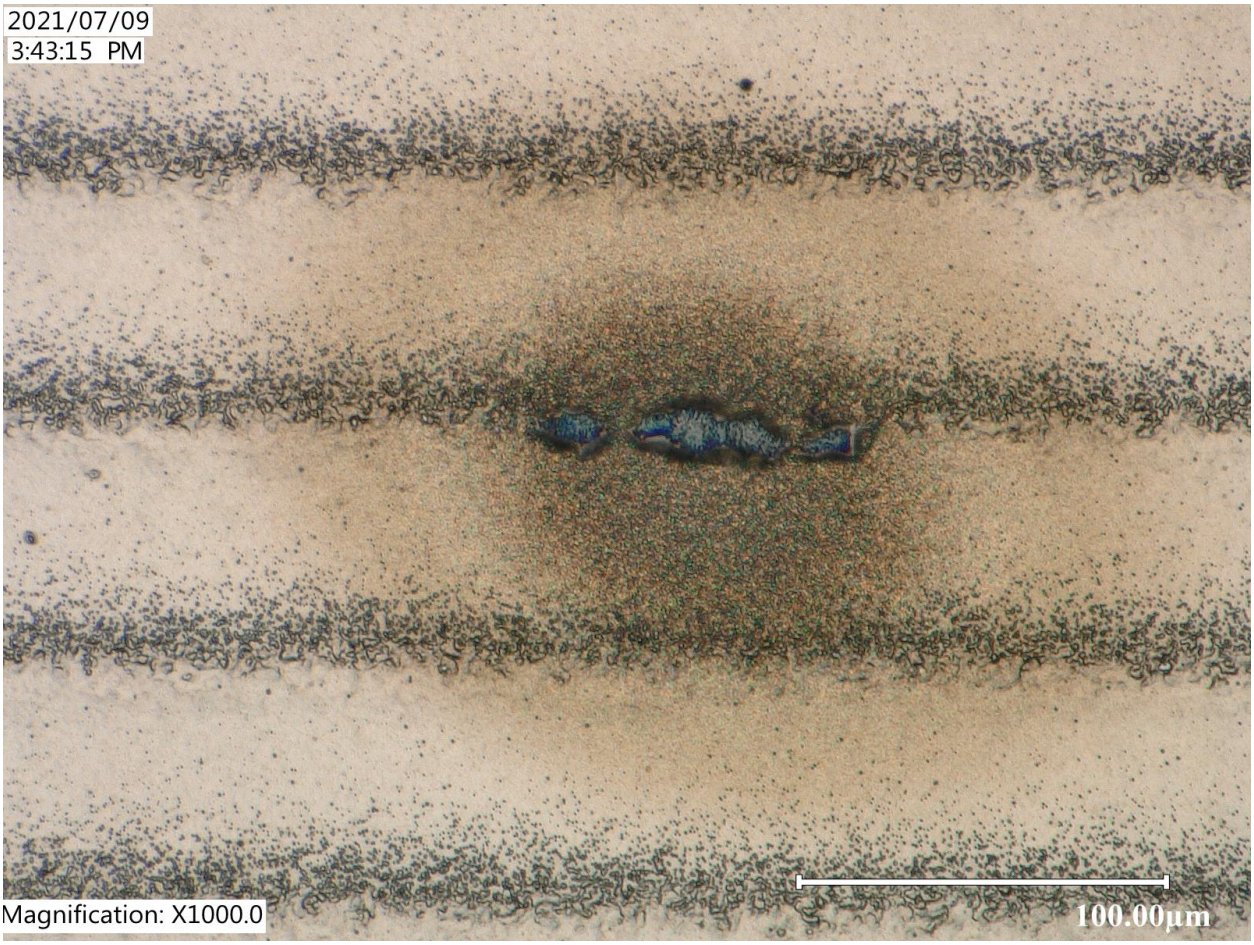

Sample 029 – Damage at 14 µJ

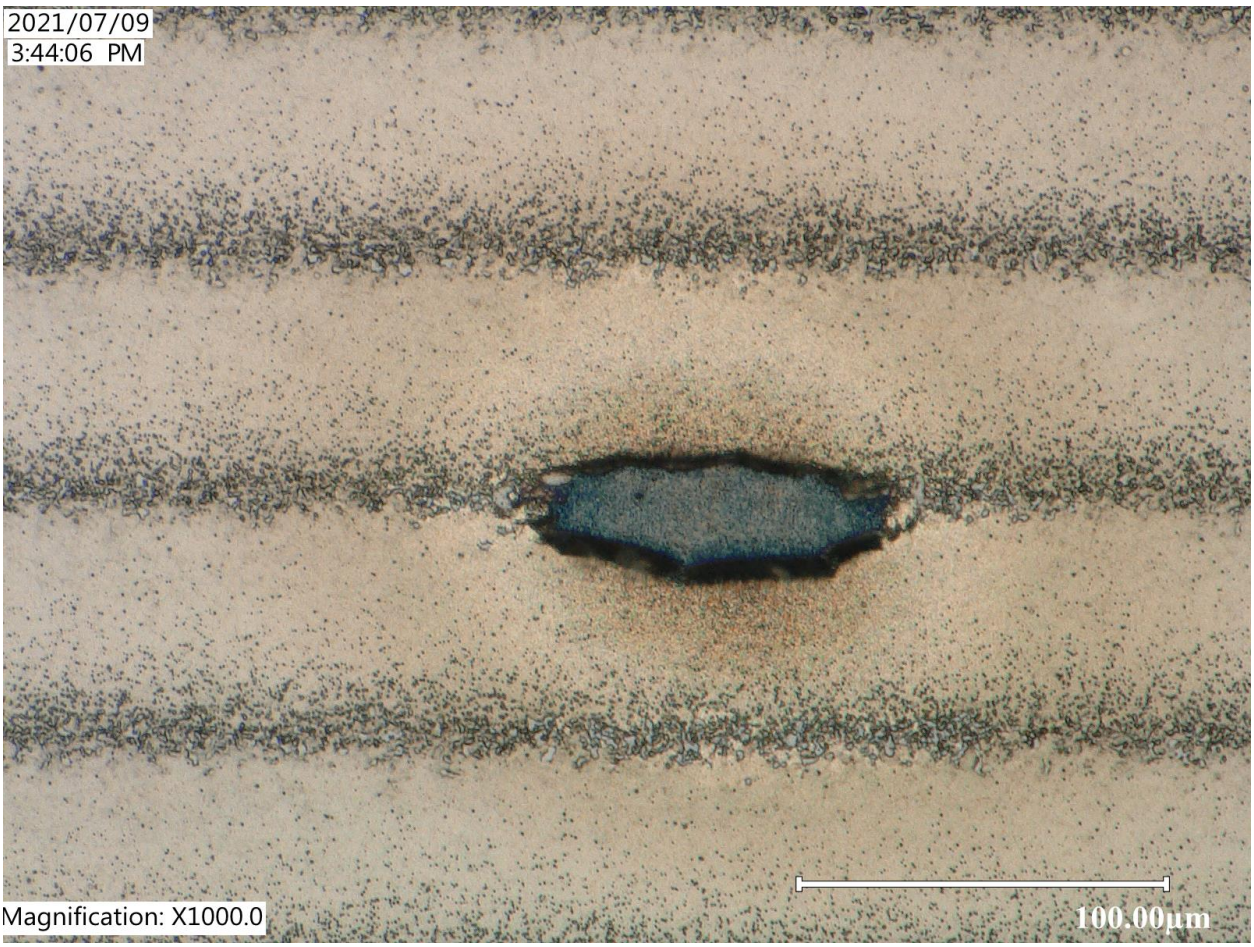

Sample 030 – Damage at 14 µJ

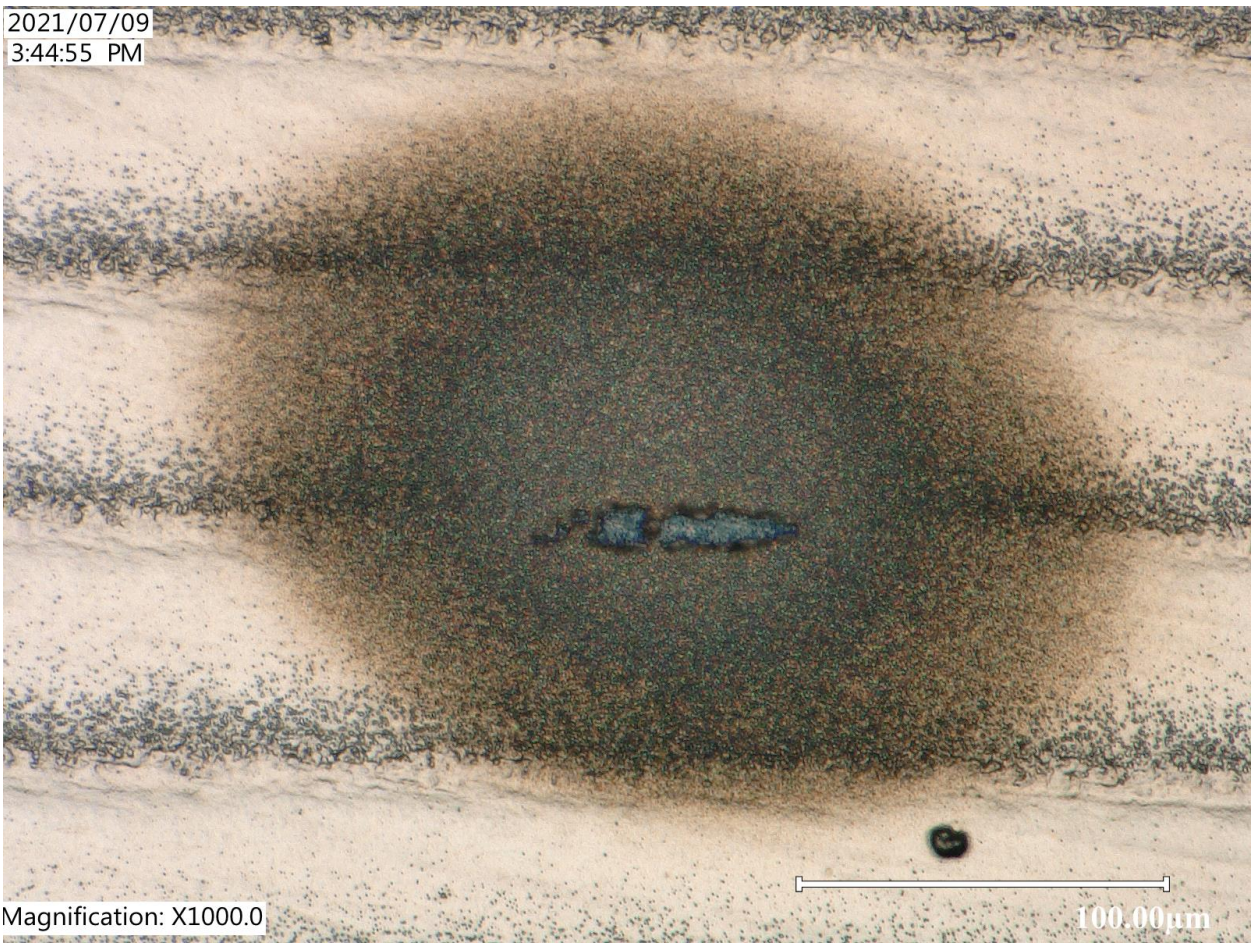

Sample 031 – Damage at 8 µJ

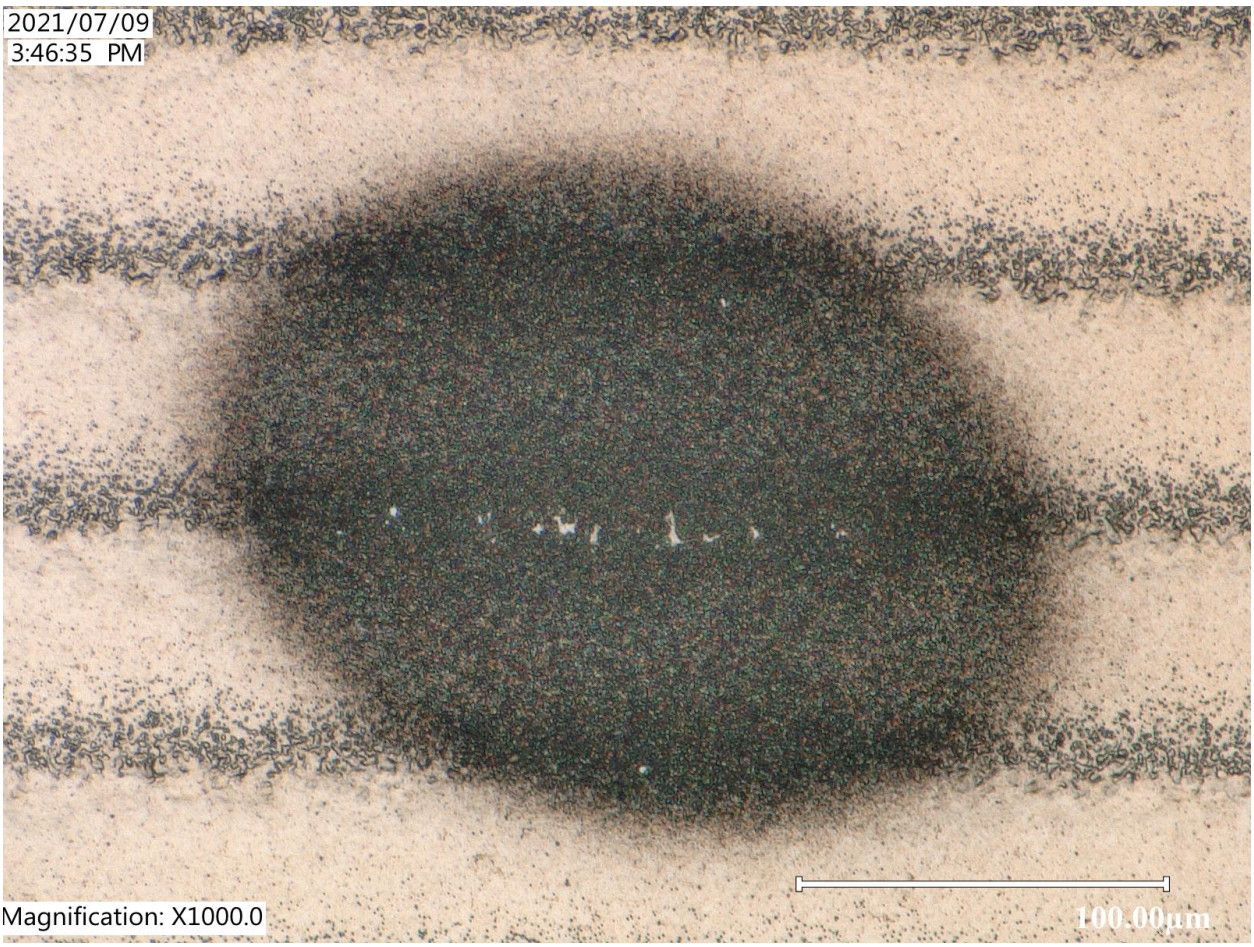

Sample 032 – Damage at 10 µJ

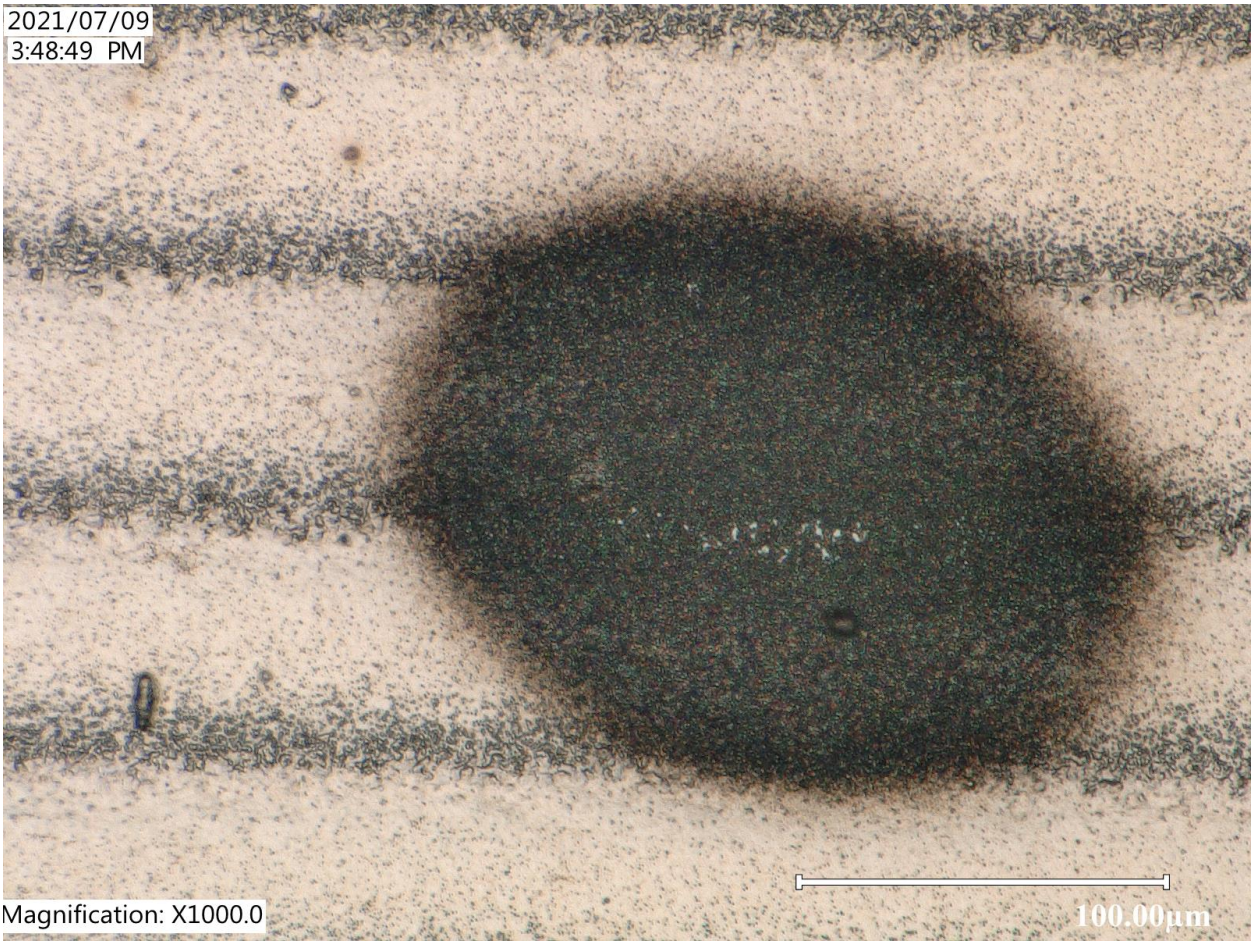

Sample 033 – Damage at 12 µJ

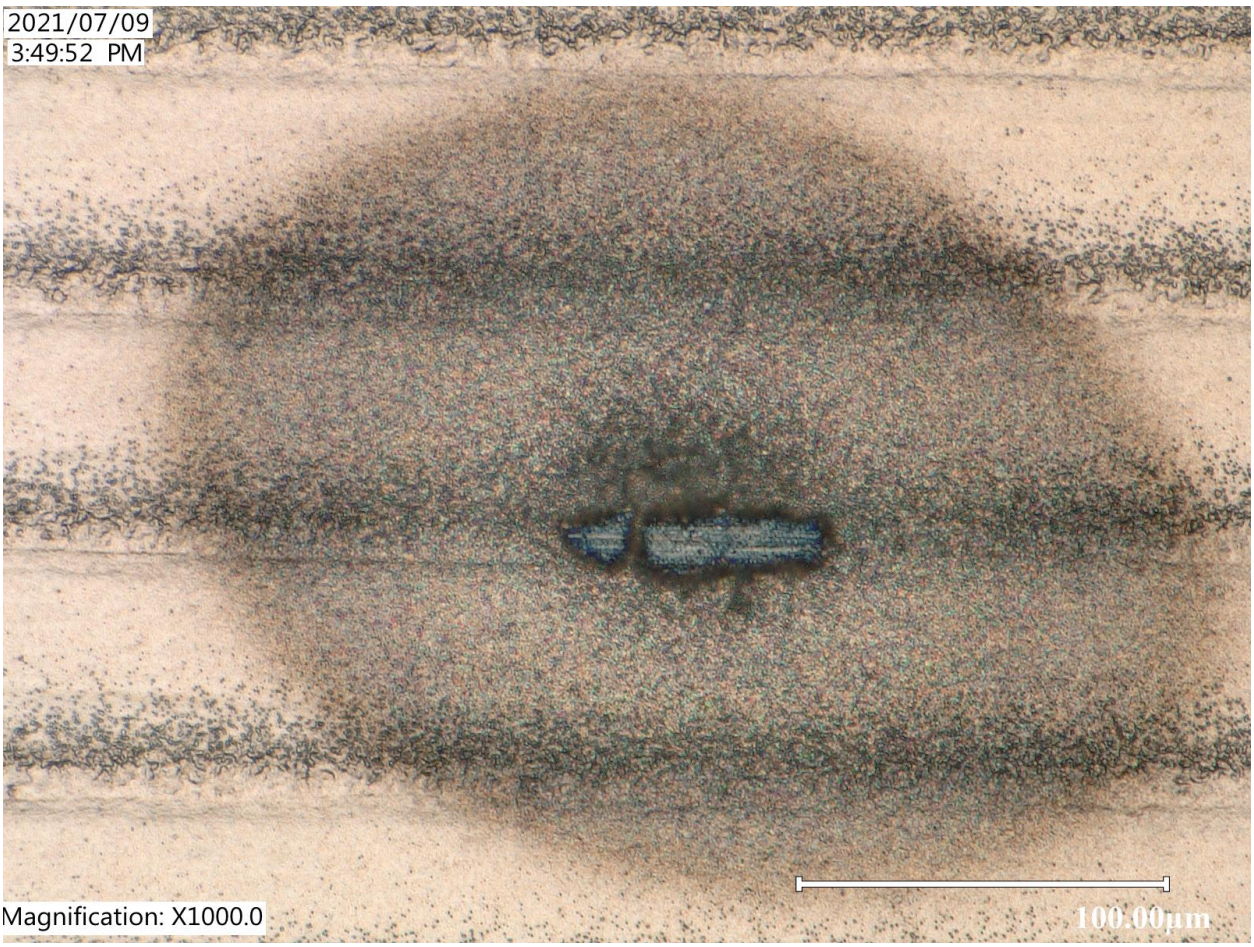

Sample 034 – No damage at 14 µJ

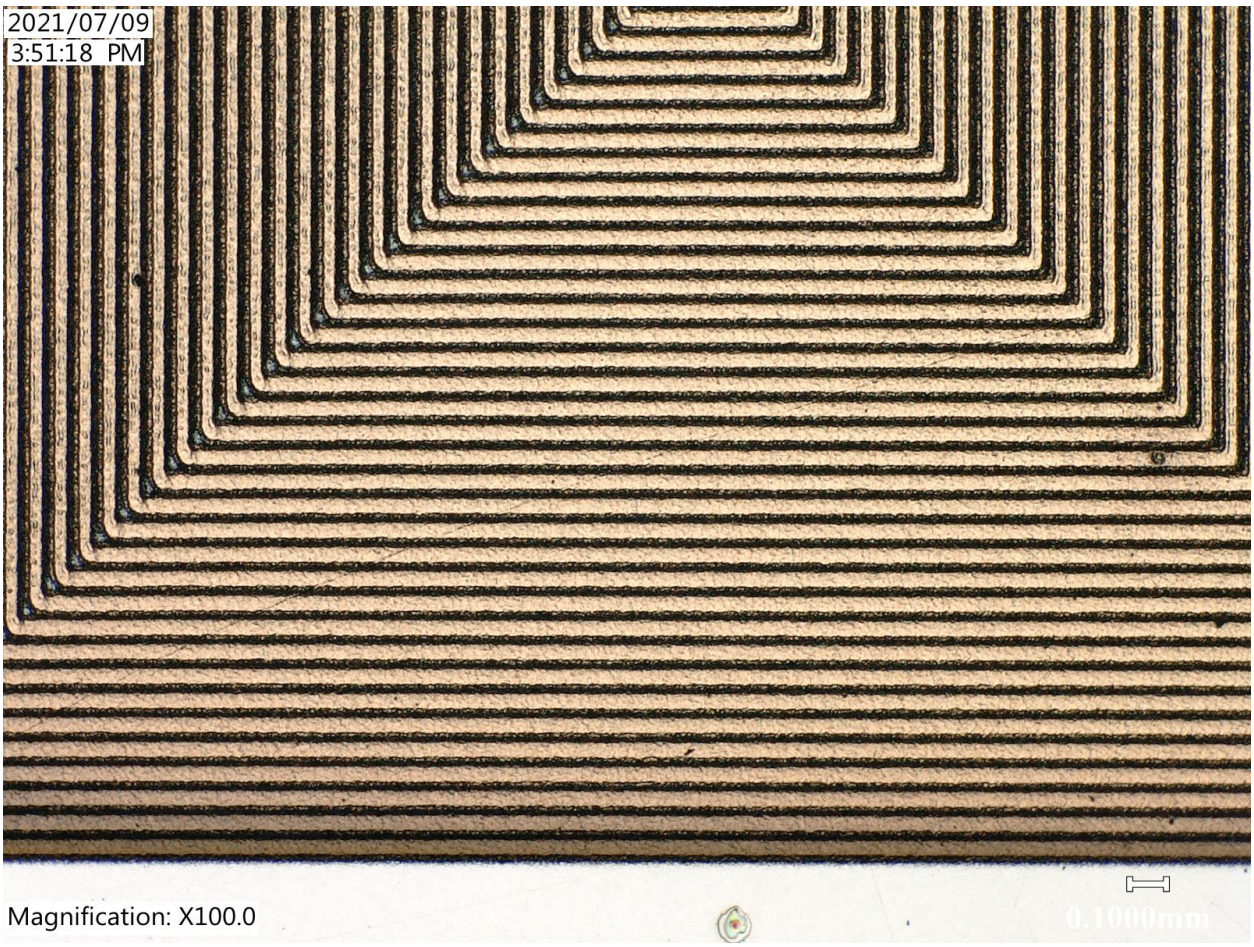

Sample 035 – No damage at 14 µJ

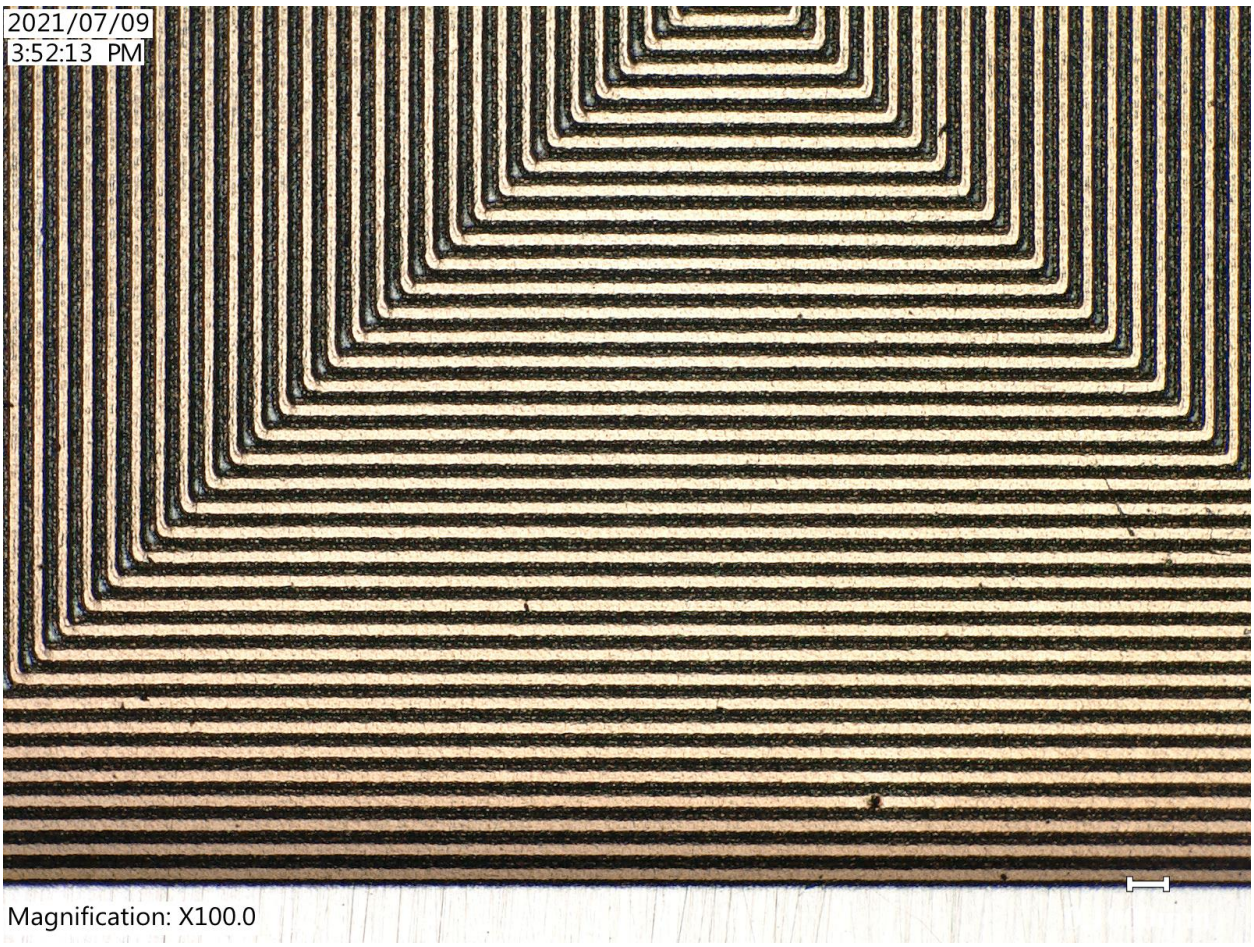

Sample 036 – No damage at 14 µJ